Effects of Membrane Potential on the Capacitance of Skeletal Muscle Fibers

MARTIN F. SCHNEIDER and W. KNOX CHANDLER

From the Department of Physiology, Yale University Medical School, New Haven, Connecticut 06510. Dr. Schneider's present address is the Department of Physiology, University of Rochester School of Medicine and Dentistry, Rochester, New York 14642.

ABSTRACT A method for measuring muscle fiber capacitance using small test pulses applied with the three-microelectrode voltage clamp is presented. Using this method, three membrane potential-dependent changes in capacitance were observed: (*a*) Capacitance of polarized fibers increased by 5–15% with depolarization from $V < -100$ mV to voltages slightly below the contraction threshold. (*b*) Capacitance of fibers depolarized to −30 mV by 100 mM Rb solution decreased by roughly 8% with further depolarization to about +50 mV and increased with repolarization, exhibiting a maximum increase of about 10% at −80 to −90 mV. (*c*) Capacitance of fibers depolarized to −15 mV by 100 mM K solution increased by about 19% with further depolarization to +43 mV and decreased by about 23% with repolarization to −62 mV. Effects *a* and *b* are attributed to changes in specific membrane capacitance due to voltage-dependent redistribution of mobile charged groups within surface or T-tubule membranes. Effect *c* is caused by changes in the T-system space constant λ_T due to the voltage dependence of K conductance (inward rectification). Analysis of *c* showed that in 100 mM K solution $\lambda_T \simeq 30$ μm when inward rectification was fully activated by hyperpolarization and that the density of inward rectifier channels is about the same in surface and tubular membranes. Fiber internal resistance was found to be independent of voltage, a necessary condition for the interpretation of the capacitance measurements.

INTRODUCTION

The electrical capacitance of skeletal muscle fibers, when referred to a unit area of fiber surface membrane, is several times greater than 1 μF/cm^2 (Katz, 1948; Fatt and Katz, 1951), the value considered to be characteristic of biological membranes (cf. Cole, 1968). Applying AC cable analysis, Falk and Fatt (1964) showed that the large capacitance could be attributed to the presence of two capacitors in parallel, one with and the other without a series resistance. The capacitance without series resistance was identified with the surface membrane whereas the capacitance with series resistance was assigned to the membranes of the traverse tubular system. Subsequent analysis (Schneider, 1970; Valdiosera et al., 1974 *b*) revealed that the T-system contribution was more accurately represented using a model in which the T-tubule membrane resistance and capacitance were distributed along the radially oriented T-system luminal resistance.

If the distributed model of the T system is valid, a step of voltage applied across the fiber surface should decrease as it spreads radially into the tubular network. Since the amount of decrement is a function of the T-system electrical space constant λ_T, the apparent capacitance of the T system should also be a function of λ_T. For example, if λ_T were small compared with fiber radius, the change in tubular potential near the center of the fiber would be smaller than the change near the surface. As a result the central portion of the tubular capacitance would be less charged than the peripheral portion. On the other hand, if λ_T were large, the tubular membranes would be more uniformly charged and the apparent value of tubular capacitance would be greater.

The influence of λ_T on tubular capacitance can be demonstrated by measuring fiber capacitance under conditions in which λ_T is altered. One way of changing λ_T is to vary the conductance of the inwardly rectifying potassium channels (Katz, 1949), at least some of which are localized in the T-system membrane (Hodgkin and Horowicz, 1960; Almers, 1972 *b*). By comparing capacitance measurements made when inward rectification is turned either off by depolarization or on by hyperpolarization it should be possible to detect voltage-dependent changes in capacitance arising from changes in λ_T. The results presented here substantiate this prediction and show that capacitance measurements may provide a useful way to localize permeability changes as being surface or tubular in origin. λ_T-dependent changes in capacitance have also been demonstrated by Adrian and Almers (1974) who varied λ_T by altering the luminal conductivity of the T system.

During the course of these experiments it was found that even under conditions in which λ_T was large there were still changes in capacitance associated with changes in voltage. Because of its possible importance in excitation-contraction coupling, the extra charge movement corresponding to the voltage-dependent capacitance has been analyzed in detail, for the most part using fibers in which contraction was blocked by hypertonic sucrose solutions (Schneider and Chandler, 1973; Almers, 1975; Chandler et al., 1975; Chandler et al., 1976 *a* and *b*; Adrian and Almers, 1976 *a*, *b*; Almers, 1976). The results reported here show that the charge movement phenomenon described in hypertonic solutions is also present in isotonic solutions and that it can be detected below the contraction threshold as a voltage-dependent change in capacitance. In addition, capacitance measurements in depolarized fibers revealed the presence of a second system of membrane charges which exhibit properties different from the originally described charge movement system.

METHODS

Frog sartorius muscles were dissected out and stretched to 1.3 times slack length over a raised pedestal in a Lucite chamber. Individual muscle fibers were voltage clamped at their pelvic ends using the three-microelectrode technique of Adrian et al. (1970 *a*). Two microelectrodes, inserted at distances ℓ and 2ℓ from the end of a fiber, were used to monitor the respective voltages V_1 and V_2 (Fig. 1). A third microelectrode, inserted a distance ℓ' from the V_2 electrode was used for passing current. The voltage-monitoring electrodes were filled with 3 M KCl and had tip potentials of less than 5 mV. Current-

passing electrodes were filled with 2 M potassium citrate. Microelectrode resistances ranged from 5 to 12 mΩ except in the experiments designed to study the voltage dependence of r_i when 10–20-MΩ electrodes were used. Electrodes for measuring V_1 and V_2 were selected to have the same resistance.

With this electrode arrangement and for ℓ sufficiently small compared to the fiber space constant, Adrian et al. (1970 *a*, Equation 1) have shown that i_m, the membrane current density per unit length of fiber at the V_1 electrode, is closely approximated by

$$i_m \simeq \frac{2\Delta V}{3\ell^2 r_i}, \tag{1}$$

where ΔV is the difference in potential $V_2 - V_1$ recorded by the two microelectrodes. A purely resistive internal impedance (Mobley et al., 1974 and 1975) is required for Eq. 1 and all subsequent equations dealing with voltage transients recorded using the three-microelectrode method.

The fiber space constant λ and internal resistance per unit length r_i are related to the steady levels $\Delta V(\infty)$, $V_1(\infty)$, and $I(\infty)$ of ΔV, V_1, and applied current by the equations

$$\lambda \simeq \left[\frac{3\ell^2 V_1(\infty)}{2\Delta V(\infty)}\right]^{1/2} \tag{2}$$

and

$$r_i = \frac{V_1(\infty)\cosh[(2\ell + \ell')/\lambda]\{1 + \tanh[(2\ell + \ell')/\lambda]\}}{\lambda I(\infty)\cosh(\ell/\lambda)}, \tag{3}$$

(Adrian et al., 1970 *a*). Since λ and r_i were measured using small pulses applied from the holding potential, $\Delta V(\infty)$, $V_1(\infty)$, and $I(\infty)$ in Eqs. 2 and 3 refer to changes from the values at the holding potential. The value of r_i for each fiber was used to calculate its apparent radius a by assuming a circular fiber cross section and using the internal resistivity given by Hodgkin and Nakajima (1972 *a*). The values of a were used to convert measurements of conductance or capacitance per unit fiber length to conductance or capacitance per unit area of fiber surface.

The voltage clamp circuit (Fig. 1) consisted of a Tektronix 502 oscilloscope amplifier (Tektronix, Inc., Beaverton, Ore.) followed by a ±100-V output operational amplifier (Analog Devices model 170, Analog Devices, Inc., Norwood, Mass.). The latter was operated at a closed loop DC gain of 6 with diode limiters in its input circuit to prevent saturation. The overall DC clamp gain was determined by the gain setting of the 502 amplifier and was usually 12,000 or 24,000. The feedback capacitance C_2 (Fig. 1) was adjusted so as to allow maximum DC gain without oscillation.

The controlled voltage was the membrane potential at $x = 2\ell$, determined as the difference between V_2 and V_3, V_3 being the voltage recorded by a third voltage-monitoring microelectrode positioned just outside the fiber between the V_1 and V_2 electrodes (Fig. 1). Since the bath was held at virtual ground (Analog Devices model 49 amplifier) V_3 was close to zero except during the make and break of a voltage step when a signal of 5–30 mV could be recorded. Because of the 1-MΩ input resistance at each terminal of the 502 amplifier and the summing circuit at the negative terminal (Fig. 1), the voltage controlled was actually $V_2 - 0.97\ V_3$. The holding potential V_H was set equal to the membrane potential recorded when the V_2 electrode was initially inserted.

By controlling $V_2 - V_3$ rather than $V_1 - V_3$, clamp stability was improved and the size of voltage transients near the current electrode was decreased. For purposes of determining λ, r_i, or fiber capacitance either $V_2 - V_3$ or $V_1 - V_3$ could have been used as the controlled

voltage since λ and r_i calculations depend only on steady-state measurements (Eqs. 2 and 3) and the capacitance determination is independent of the time-course of the applied voltage providing that both V_1 and V_2 reach steady levels (Appendix B).

Command pulses V_c were applied to the 502 input via a summing network using capacitance C_1 to introduce an exponential delay (Fig. 1). C_1 was adjusted to give the most rapid recorded clamp step which appeared to be exponential; the time constant usually used was 10–30 μs. Voltages were monitored using unity gain FET input amplifiers (Department of Physiology electronics shop) with driven shields around the electrodes to minimize capacitance to ground. The amplifiers had a measured input capacitance of about 1 pF which together with an electrode to bath capacitance of less than 0.5 pF gives an expected time constant of less than 7.5–18 μs for 5–12-MΩ electrodes.

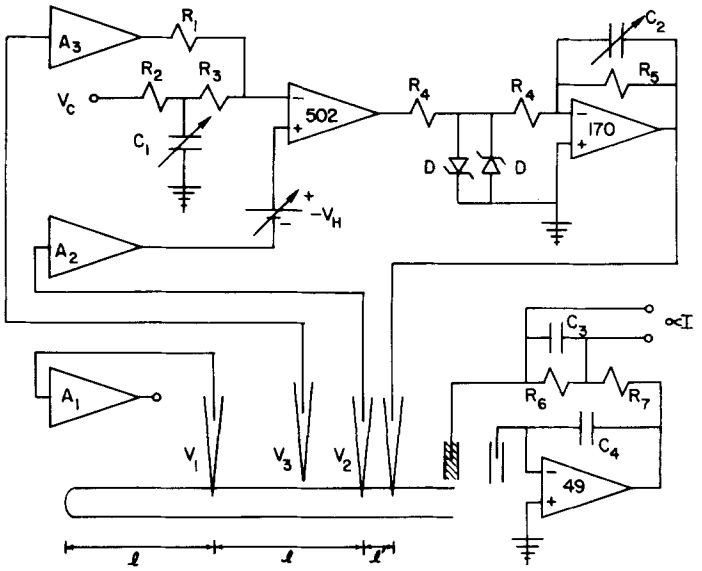

FIGURE 1. Circuit for muscle voltage clamp and circuit for holding the bath at ground and recording total applied current. Amplifiers A_1, A_2, and A_3 were unity gain FET input voltage followers. Operational amplifiers 170 and 49 were Analog Devices amplifiers having those numbers. Amplifier 502 is the vertical amplifier of a Tektronix 502 oscilloscope. Resistance values were (KΩ) 10 (R_1), 100 (R_2), 417 (R_3), 3.3 (R_4), 41 (R_5), 50 (R_6), and 0.33 (R_7); capacitance values were (pF) 50–680 (C_1), 20–400 (C_2), 25 (C_3), and 10 (C_4). The two diodes (D) were made using 2N4916 transistors, connected as Zener diodes. See text for detailed description.

The current-passing electrode was carefully covered with a grounded shield which extended to within a fraction of a millimeter from the bathing solution. The level of solution was adjusted so that there was only a shallow layer above the muscle. $I(\infty)$ was monitored as a voltage drop across a 50-KΩ resistor (R_6) in the feedback loop of the bath amplifier.

As will be described in the Theory section, capacitance measurements were based on the amount of charge carried by transient capacitative charging currents. Since charge carried by a current is given by its integral over time, ΔV signals were digitally integrated on line and the results stored for subsequent calculations. A computer of average transients (Technical Measurement Corporation CAT 1000) carried out the integration

by means of a linear voltage to frequency (V to f) converter and a digital pulse counter. Each integration period corresponded to the interval between externally applied timing pulses. The dead time between successive intervals was about 15 μs and the intervals used varied from 2.5 to 12 ms, depending on electrode separation. In the special experiments designed to investigate the voltage dependence of r_i, 48-ms counting intervals were employed to measure steady levels of ΔV, V_2, or I. Timing pulses as well as the clamp command pulse durations were set with a digital pulse generator designed by Mr. Harry Fein and constructed in the Department of Physiology electronics shop.

In general three counting intervals were used to determine a base line before the start of a test pulse. The start of the fourth counting interval corresponded to the "on" of the test pulse and the start of the 11th interval corresponded to the test pulse "off." A total of 17 intervals were generally used. The ΔV integrals measured during the first three intervals after the pulse on or off were used to determine the transient current; the integrals for the three succeeding intervals were used to measure steady current levels.

V to f conversion and counting were also used to measure V_2 and $I(\infty)$. Since only one counter was available, ΔV, V_2, and $I(\infty)$ determinations had to be made on different sweeps. During each sweep the desired signal was applied to the input of a 3A9 plug-in amplifier in a Tektronix 565 oscilloscope and the 3A9 output (~1-V/cm deflection) was used as the input to the CAT 1000. The general sequence of an experiment was to first monitor ΔV for several sweeps using positive or negative pulses of amplitude 10 mV or less applied from the holding potential. Then $I(\infty)$ was monitored on repeat sweeps using the same pulses. These data were used for calculating the cable parameters λ and r_i. Next, ΔV was monitored for a series of small test pulses superimposed on different prepulse voltage levels. Then, the ΔV and $I(\infty)$ sweeps to be used for the cable analysis were repeated. Finally, V_2 was monitored for test pulses at all prepulse levels used for ΔV measurements. In 14 cases V_2 measurements were made at the start and end of a run and found to agree within 0.4% (mean absolute difference = 0.2%) for the same prepulse test pulse values.

Test pulses were applied 90–100 ms after the start of the prepulse, except in the case of the experiments in 100 mM Rb solution where the test pulses were given about 500 ms after the start of the prepulse.

The second beam of the 565 oscilloscope was driven by a 3A3 plug-in amplifier and was used to display V_2 and ΔV on a slower time base so that both the prepulse and test pulse could be observed. All sweeps were photographed. Clamp stability was checked both during the experiment and subsequently from photographs. V_2 and ΔV were continuously monitored on a strip chart recorder (Brush model 280).

The solutions used were isotonic and had the compositions listed in Table I. Muscles studied in solution C or D (100 mM K or Rb, Cl-free SO_4 solutions) were first soaked in solution E for times ranging from 11 min to over an hour for washout of external Cl. They were then soaked in the experimental solution for at least 50 min before any measurements were made. The bath temperature was monitored using a thermistor and was held at a constant level between 0 and 3°C or between 16 and 18°C using a Peltier cooling device (Cambion).

The initial experiments in the investigation were carried out using sartorius muscles from *Rana pipiens*. Later, *Rana temporaria* were used, mainly because they have larger fibers and because the pelvic ends of the fibers insert more uniformly into the tendon. The latter property is important for the three-microelectrode technique since it allows the position of the end of a particular fiber to be determined reliably. The experiments on capacitance which are presented in this and the following paper were done in March through June, 1972, using *R. temporaria*. Similar results were obtained from *R. pipiens*. The experiments on the voltage dependence of r_i were done in March using *R. pipiens*.

THEORY

Capacitance Measurements Using the Three-Microelectrode Voltage Clamp

The lumped circuit illustrated in Fig. 2 A represents a good first approximation to the equivalent circuit for voltage recording using the three-microelectrode voltage clamp. Since $r_i\ell$ is the internal resistance separating the V_2 and V_1 electrodes, $\Delta V/r_i\ell$ serves as an approximation to the longitudinal current midway between voltage electrodes. Because this current must exit over a length $3\ell/2$ of fiber, from the midway point to the end of the fiber, the element $r_i\ell$ in Fig. 2 A is placed in series with the admittance $3\ell y_m/2$ of that length of fiber. A circuit for y_m, the admittance per unit fiber length connecting fiber interior with the external bathing solution, is given in Fig. 2 B. The purely conductive and capacitative elements g_m and c_m' represent the effective conductance of surface membrane and T system in parallel and the capacitance of the surface membrane. Like

TABLE I

IONIC COMPOSITION OF SOLUTIONS

Solution	Rb	K	Na	TEA	Ca	Cl	SO_4*	Buffer
	mM	*mM*	*mM*	*mM*	*mM*	*mM*	*mM*	*mM*
A	5	—	117.5	—	1.8	136.1	—	Tris‡
B	5	—	—	117.5	1.8	136.1	—	Tris‡
C	100	—	92.6	—	*	—	93.8	Phosphate
D	—	100	92.6	—	*	—	93.8	Phosphate
E	—	5	187.5	—	*	—	93.8	Phosphate
F	5	—	187.5	—	*	—	91.2	Phosphate

* In addition to the SO_4 added as Rb, K, or Na salt, solutions C and D contained 8.4 mM $CaSO_4$ and solutions E and F contained 8.8 mM $CaSO_4$ (cf. Hodgkin and Horowicz, 1959). SO_4 from $CaSO_4$ has not been included in the listed concentrations.

‡ Tris indicates 1.0 mM Tris-acid maleate buffer, pH 7.1 (Gomori, 1955). The phosphate buffer contained 2.15 mM $HOP_4^=$, 0.85 mM $H_2PO_4^-$ (pH 7.0). Solutions A, B, and F contained 10^{-6} g/ml tetrodotoxin.

all circuit elements of y_m, the elements g_m and c_m' correspond to a unit length of muscle fiber. It should be noted that a given circuit element in Fig. 2 B does not represent the resistance or capacitance of a particular part of the T system or surface membrane but rather that the entire circuit has an admittance equal to that of the T system in parallel with the surface membrane. Thus, for example, the DC contributions of both the T system and surface membrane have been included in g_m. Use of a single series RC element to represent the T-system transient current path would reduce y_m to the lumped circuit proposed by Falk and Fatt (1964). To represent the distributed nature of the T system (Schneider, 1970) it is necessary to use an infinite number of series RC elements in y_m (Adrian et al., 1969). In general, y_m represents one equivalent circuit for a two-terminal network having any number of time constants depending on the number and nature of the series RC elements.

Many other two-terminal circuits are electrically equivalent to y_m for all measurements made between the two terminals. The circuit chosen for y_m (Fig. 2 B) has the property that its effective capacitance c_{eff}, which is determined by measuring capacitative current in the external circuit, must equal the sum of all capacitances in y_m. In other equivalent circuits, in which some capacitors have finite shunt resistors as well as nonzero series resistors, c_{eff} would be less than the sum of all capacitances in the circuit. The present objective is to

develop the method for measuring c_{eff}. Its significance in terms of the actual capacitance of various fiber membrane systems will be dealt with in the next section.

Voltage clamp records *a* through *d* of Fig. 3 were recorded from a muscle fiber, but for purposes of illustration can be considered as responses of the lumped circuit (Fig. 2 A). A voltage step at V_2 (record *a*) results in a slower change in potential at the V_1 electrode

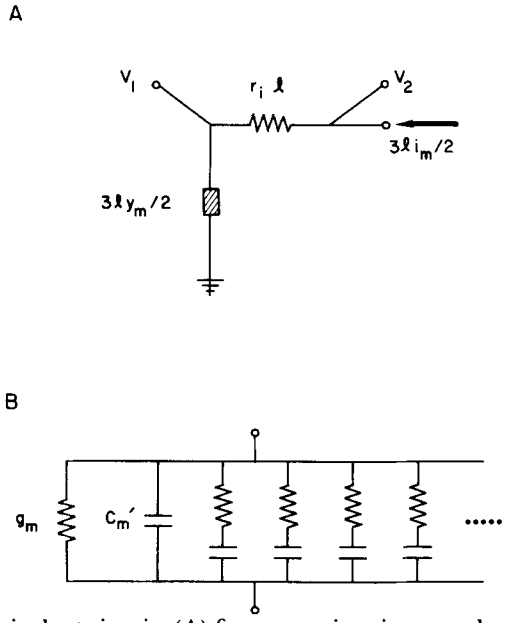

FIGURE 2. Equivalent circuits (A) for approximating membrane current using the voltage difference between V_2 and V_1 and (B) for the admittance y_m of a unit length of muscle fiber. (A) The current leaving the fiber from a point midway between voltage electrodes to the end of the fiber (i.e., over a length $3\ell/2$) crosses an admittance $3\ell y_m/2$. It is equal to the longitudinal current midway between voltage electrodes, which is approximated as the voltage drop $\Delta V(= V_2 - V_1)$ between the two microelectrodes divided by the longitudinal resistance $r_i\ell$ separating the two electrodes. If the terminal $3\ell/2$ of fiber were isopotential, $\Delta V/r_i\ell$ would be equal to $3\ell/2$ times the current i_m per unit fiber length at the V_1 electrode. This is the current shown entering the approximate equivalent circuit. See text for further details. (B) The admittance y_m of a unit length of fiber is given by the parallel placement of the total conductance g_m, the surface membrane capacitance c_m', and the equivalent circuit for the transient current path through the T system. The latter is represented by a number of series RC elements connected in parallel. The nature and number of these series RC paths depends on the model used to represent the T system (see text).

(record *b*). The current flowing between the V_2 and V_1 electrodes, $\Delta V/r_i\ell$, is proportional to the amplitude of record *d* and is equal to the ionic current through $3\ell g_m/2$ plus the sum of all capacitative currents crossing $3\ell y_m/2$. y_m is the admittance of the circuit in Fig. 2 B. As the capacitors become charged the capacitative current declines to zero and ΔV reaches a steady level $\Delta V(\infty)$ (record *d*). The steady longitudinal current $\Delta V(\infty)/r_i\ell$ corresponds to the steady-state membrane ionic current. If the fiber membrane conduct-

ance remains constant during the pulse, the membrane ionic current must at all times be proportional to V_1. Consequently, the component of longitudinal current which leaves the fiber in the form of ionic current is given by $(\Delta V(\infty)/r_i\ell)\ (V_1/V_1(\infty))$.

Taking the difference between total and ionic currents and dividing by $3\ell/2$ gives the equation

$$i_c \simeq 2\left(\Delta V - \frac{V_1}{V_1(\infty)}\Delta V(\infty)\right)/3\ell^2 r_i \tag{4}$$

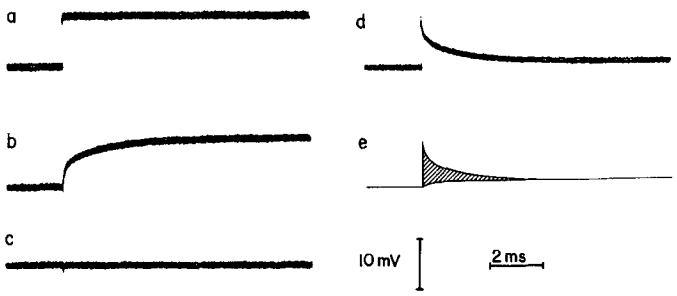

FIGURE 3. Voltage records obtained from a muscle fiber using the three-microelectrode voltage clamp to apply a step change in potential at the V_2 electrode. Records *a* through *d* correspond to oscilloscope photographs of the following signals (see Fig. 1): (*a*) $V_2 - V_3$; (*b*) $V_1 - V_3$; (*c*) the same as *b* but with the V_1 electrode positioned just outside the fiber; (*d*) $V_2 - V_1$ (= ΔV). The small size of the artifact in record *c* indicates that voltage pickup by the microelectrodes and voltage gradients in the bath introduced minimal error into the recorded voltages. The amplitude of the ΔV record, redrawn as the upper line in *e*, is approximately proportional to the membrane current at the V_1 electrode. The ionic current component in ΔV is proportional to V_1 scaled as in the lower line in *e*. The area between the upper and lower lines in *e* is proportional to the charge carried by the capacitative current. See text for further details. Fiber 101.2, solution B, 1.7°C. ℓ = 372 μm, ℓ' = 28 μm; the proportionality factor $2/3\ell^2 r_i$ between ΔV and i_m is 98 nA/(mV cm).

for the capacitative current i_c per unit fiber length. Approximate equality is indicated since the lumped circuit represents only an approximation to the distributed nature of the terminated segment (Appendix B). c_{eff} is equal to the total charge per unit length of fiber carried by the capacitative current divided by $V_1(\infty)$. It is approximately proportional to the shaded area in Fig. 3 *e* and is given by

$$c_{\text{eff}} \simeq \frac{2}{3\ell^2 r_i V_1(\infty)} \int_0^{t_1} \Delta V_{\text{tr}}\, dt, \tag{5}$$

where the transient component ΔV_{tr} of ΔV is given by $\Delta V - (V_1 \Delta V(\infty)/V_1(\infty))$. t_1 is a time by which V_1 and ΔV have reached their steady levels and $t = 0$ corresponds to the start of the applied voltage change. Experimentally the steady levels of ΔV and V_1 used in Eq. 5 were evaluated by integrating the respective signals from t_1 to $2t_1$ and dividing by t_1. Since capacitance measurements were made using test pulses from various prepulse voltages, changes in ΔV and V_1 from prepulse levels were used to calculate c_{eff}. This procedure is justified by the superposition theorem, providing that g_m (Fig. 2 B) is unchanged by the test pulse.

The complete cable analysis for the terminated segment (Appendix B) reveals that the approximate expression for c_{eff} (Eq. 5) can be made exact by introducing the correction factor $h(\ell/\lambda)$,

$$c_{eff} = \frac{2h(\ell/\lambda)}{3\ell^2 r_i V_1(\infty)} \int_0^{t_1} \Delta V_{tr}\, dt. \tag{6}$$

The function $h(\ell/\lambda)$ depends on the values of ℓ/λ and of the parameter K. $K = r_i\ell/r_1$, where r_1 is the leak resistance at the site of insertion of the V_1 electrode (Appendix B). Fig. 4 presents graphs of $h(\ell/\lambda)$ for infinite r_1 ($K = 0$, upper curve) and for $K = 0.1$ (lower curve), the upper limit for K calculated as described in Appendix A. For $\ell/\lambda < 0.7$, as was the case for all capacitance measurements, $0.99 < h(\ell/\lambda) < 1.05$.

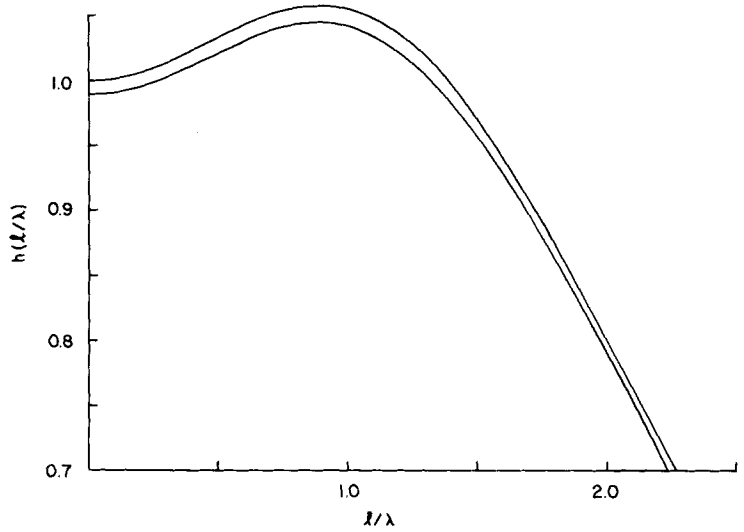

FIGURE 4. Graphs of the function $h(\ell/\lambda)$ which makes the approximate Eq. 5 for calculating fiber capacitance an exact Eq. 6. The upper curve corresponds to infinite leak resistance r_1 at the V_1 electrode, Eq. 18 *b*. The lower curve was calculated according to Eq. 22 *b* with $K = 0.1$. K is given by $r_i\ell/r_1$. See text and Appendix B for details.

In practice $h(\ell/\lambda)$ was calculated assuming infinite r_1 (Eq. 8 *b*) and c_{eff} was calculated from Eq. 6. The error introduced into the calculation of $h(\ell/\lambda)$ by assuming infinite r_1 is discussed in Appendix B and for the present experiments was at most 2.5%.

An integral analysis similar to that presented here has been used by Adrian and Almers (1974) to derive equations for calculating fiber capacitance. In their case c_{eff} was calculated from records of total current applied to a fiber voltage clamped at a point midway along its length. A disadvantage of the total current method is that the calculated capacitance is strongly dependent on the measured value of λ. In the case of the three-electrode clamp at the end of a fiber, λ measurements have only a minor influence on c_{eff} through their effect on $h(\ell/\lambda)$.

Two properties of the three-microelectrode method of capacitance measurement make it advantageous for use with muscle fibers. First, the exact time-course of the imposed potential change at V_2 is unimportant (Appendix B); the only requirements are that the

recording delays introduced by amplifiers A_1 and A_2 and their respective microelectrodes (Fig. 1) be similar and that both the V_1 and V_2 signals reach steady levels at time t_1. Second, leak conductances at the sites of microelectrode insertion have little effect on the measurement of $r_i c_{eff}$. Leak conductances at the V_2 and I electrodes would clearly have no effect (see Appendix A). As mentioned above and discussed in Appendix B, a leak conductance at the V_1 electrode would influence $r_i c_{eff}$ through the choice of $h(\ell/\lambda)$, but the effect is minimal.

Electrode leak conductances at all three electrodes introduce errors into the measurement of r_i (Appendix A) and, consequently, into the calculation of c_{eff} (Eq. 6). However, if r_i is independent of V and if all values of capacitance are expressed relative to the capacitance measured at some reference voltage, any error due to r_i will be cancelled.

A possible source of error in the capacitance measurement is the presence of extracellular potential differences. The extracellular potential due to capacitative current crossing either the wall of the current electrode or the fiber itself decreases with distance from the current-passing electrode (Valdiosera et al. 1974 *a*). Thus V_2 may include a larger component of extracellular potential at the make and break of the pulse than V_1, giving rise to an error in ΔV. Since the time-course of the difference in external potentials at the V_2 and V_1 electrodes is probably similar to the time-course of V_1-V_3 with V_1 outside the fiber (Fig. 3 *c*), it seems safe to assume that the extracellular potential change was sufficiently rapid so as to introduce little error into the ΔV integral.

Deviations from one-dimensional cable behavior due to three-dimensional spread of current inside the fiber away from the tip of the current electrode (Falk and Fatt, 1964; Eisenberg and Johnson, 1970) would not be expected to introduce voltage-dependent errors into measurements of $r_i c_{eff}$ and have not been considered.

Calculation of the T-System Space Constant from Measurements of Effective Fiber Capacitance

The effective fiber capacitance, measured by integration of the charging transient, is equal to the sum of all capacitors in the equivalent circuit chosen for y_m (Fig. 2 B). This, however, is not necessarily equal to the total capacitance of surface plus T-system membranes. In the case of the distributed model of the T system, only a fraction of the total T-system capacitance contributes, with this fraction approaching unity as λ_T approaches infinity. Using the circuit in Fig. 2 B, Adrian et al. (1969) showed that the effective capacitance $c_T(a/\lambda_T)$ contributed by the T system is given by

$$c_T(a/\lambda_T) = \sum_{n=1}^{\infty} c_n, \tag{7}$$

$$c_n = 4\pi a^2 \bar{C}_W \frac{\alpha_n^2}{[(a/\lambda_T)^2 + \alpha_n^2]^2}, \tag{8}$$

where c_n is the value of the nth series capacitor in y_m. $\bar{C}_W$ is the capacitance of the T-system membrane contained in a unit volume of fiber, a is the fiber radius, and α_n is the nth root of $J_0(\alpha) = 0$. λ_T is equal to $(\bar{G}_L/\bar{G}_W)^{1/2}$, where $\bar{G}_W$ is the conductance of the T-system membranes in a unit volume of fiber and $\bar{G}_L$ is the effective T-system luminal conductance in the radial direction per unit fiber volume.

The expression for $c_T(a/\lambda_T)$, Eqs. 7 and 8, can also be given in closed form. A rather simple derivation relies on the fact that the energy stored on the capacitors in equivalent circuits containing no inductive elements must be equal (Bode, 1938). Consider first the spatially distributed model for the T system. If a voltage is applied to a muscle fiber, the energy E stored per unit fiber length on the T-system capacitance is

$$E = \frac{1}{2}\int_0^a [V(r)]^2 \bar{C}_W 2\pi r\, dr. \tag{9}$$

Here $V(r)$ denotes the potential across the T-system membrane at distance r from the fiber axis. In the steady state and for an applied voltage step $V(a)$ at the surface

$$V(r) = V(a)\frac{I_0(r/\lambda_T)}{I_0(a/\lambda_T)} \tag{10}$$

(Adrian et al., 1969. Eq. 10), where I_0 denotes a modified Bessel function. Substituting Eq. 10 into Eq. 9 and carrying out the integration gives

$$E = \frac{\pi a^2 \bar{C}_W V^2(a)}{2}\left[1 - \left\{\frac{I_1(a/\lambda_T)}{I_0(a/\lambda_T)}\right\}^2\right]. \tag{11}$$

Using the equivalent circuit of Adrian et al. (1969) for the T-system transient current path (i.e., y_m of Fig. 2 B without g_m and c_m'), the alternative expression

$$E = c_T(a/\lambda_T)V^2(a)/2 \tag{12}$$

is obtained. Equating the two expressions for E gives

$$c_T(a/\lambda_T) = \pi a^2 \bar{C}_W\left[1 - \left\{\frac{I_1(a/\lambda_T)}{I_0(a/\lambda_T)}\right\}^2\right]. \tag{13}$$

When $a/\lambda_T = 0$, $c_T(a/\lambda_T)$ measures the true total capacitance $c_T(0)$ of the amount of T-system membrane in a unit length of fiber; this is $\pi a^2 \bar{C}_W$. The ratio of effective to true T-system capacitance is thus given by

$$\frac{c_T(a/\lambda_T)}{c_T(0)} = 1 - \left\{\frac{I_1(a/\lambda_T)}{I_0(a/\lambda_T)}\right\}^2. \tag{14}$$

Using this relationship, a/λ_T can be directly determined from measurements of $c_T(a/\lambda_T)/c_T(0)$. It should be noted, however, that measured values of fiber capacitance include both surface membrane and T-system contributions; in order to use Eq. 14, the surface membrane contribution must first be subtracted from the total measured capacitances.

Checking the Voltage Dependence of r_i

The respective steady-state differential equations for membrane (i_m) and longitudinal (i) current in a one-dimensional cable are

$$i_m = -\frac{di}{dx} \tag{15}$$

and

$$i = -\frac{1}{r_i}\frac{dV}{dx} \tag{16}$$

Eqs. 15 and 16 can be combined to give

$$i\,di = \frac{i_m}{r_i}\,dV, \tag{17}$$

a generalized form of the Cole equation (Cole and Curtis, 1941). Integrating Eq. 17 in the steady state over the terminated fiber segment from fiber end ($x = 0$) to the point of insertion of the current electrode ($x = 2\ell + \ell'$) gives

$$\frac{I_S^2}{2} = \int_{V_0}^{V_{2\ell+\ell'}} \frac{i_m}{r_i}\, dV, \tag{18}$$

where I_S is the steady-state current entering the terminated or "short" fiber segment. Integrating over the infinite segment from $x = \infty$ to $x = 2\ell + \ell'$ gives

$$\frac{I_U^2}{2} = \int_{V_\infty}^{V_{2\ell+\ell'}} \frac{i_m}{r_i}\, dV, \tag{19}$$

where I_U is the steady current entering the semi-infinite or "unterminated" fiber segment. Note that by definition $I(\infty)$, the steady-state applied current, must satisfy

$$I(\infty) = I_S + I_U. \tag{20}$$

At this point it is convenient to express r_i as the product of a constant term $\bar{r}_i$ and a function $F\{V\}$ which may vary with membrane potential,

$$r_i = \bar{r}_i F\{V\}. \tag{21}$$

If $\bar{r}_i$ is chosen to be the value of r_i at a reference potential V_{ref}, $F\{V_{\text{ref}}\} = 1$. Combining Eqs. 18 through 21 and rearranging gives

$$\sqrt{\bar{r}_i} = \left[\frac{2}{I(\infty)^2}\int_{V_0}^{V_{2\ell+\ell'}} \frac{i_m}{F\{V\}}\, dV\right]^{1/2} + \left[\frac{2}{I(\infty)^2}\int_{V_\infty}^{V_{2\ell+\ell'}} \frac{i_m}{F\{V\}}\, dV\right]^{1/2}. \tag{22}$$

In order to evaluate the integrals in Eq. 22, an expression for i_m as a function of V is required. This relationship was experimentally determined by measuring the variation of ΔV with V_1 in the terminated segment. Rewriting Eq. 1 using Eq. 21 for r_i gives

$$i_m \simeq \frac{2\Delta V}{3\ell^2 \bar{r}_i F\{V\}}. \tag{23}$$

Eqs. 22 and 23 can be combined to give

$$\bar{r}_i = \left[\frac{4}{3\ell^2 I(\infty)^2}\int_{V_0}^{V_{2\ell+\ell'}} \frac{\Delta V}{F^2\{V\}}\, dV\right]^{1/2} + \left[\frac{4}{3\ell^2 I(\infty)^2}\int_{V_\infty}^{V_{2\ell+\ell'}} \frac{\Delta V}{F^2\{V\}}\, dV\right]^{1/2}. \tag{24}$$

[Since the r_i term in Eq. 1 refers to the internal resistance at a point midway between the voltage recording electrodes, $F\{V_1 + \Delta V/2\}$ rather than $F\{V_1\}$ was actually used for $F\{V\}$ in Eq. 23. Also, $F\{V\}\cdot F\{V + \Delta V/2\}$ was used rather then $F^2\{V\}$ in Eq. 24; for sake of brevity, however, the latter term is used here to denote the former product. In practice, the two were almost equal and differed slightly only for the largest depolarizations employed.]

Eq. 24 was used as a basis for testing various trial functions for $F\{V\}$ to see if they were consistent with experimental observations. The procedure for testing a given trial function involved the following steps: (*a*) The value of ΔV measured at each of a series of V_1 values was divided by the corresponding value of $F^2\{V_1\}$. (*b*) A fifth degree polynomial in V was fit to the $\Delta V/F^2\{V\}$ points. (*c*) Values of $I(\infty)$ for various voltage steps were measured in the same fiber. (*d*) Steady levels of V_0 and $V_{2\ell+\ell'}$ were calculated for each voltage step employed in (*c*) using Eq. 4 *a* for the voltage distribution in the terminated segment and Eq. 2 to calculate λ. (*e*) Using Eq. 24, and the polynomial fit for $\Delta V/F^2\{V\}$, $\bar{r}_i$ values were calculated for each voltage step at which $I(\infty)$ was measured. For the trial function $F\{V\}$ to be consistent with the data, the $\bar{r}_i$ values calculated in (*e*) would have to be the same at all voltages; if, on the other hand, the calculated $\bar{r}_i$ values varied with voltage, the trial function would be inconsistent with the observed results.

RESULTS

Muscles Bathed in 5 mM Rb Solutions

VOLTAGE-DEPENDENT CAPACITANCE IN POLARIZED FIBERS This set of experiments was concerned with fibers which had resting potentials close to the physiological range. Rb was used instead of K (solutions A and B, Table I) since Rb blocks the inward rectification and conductance "creep" which are characteristic of resting muscle K conductance (Adrian, 1964). Most measurements were made below the threshold for activating delayed rectification so that the only voltage-dependent component of fiber conductance was due to Cl (Hodgkin and Horowicz, 1959; Hutter and Noble, 1960). In solution B (Table I) TEA was used instead of Na to suppress any delayed rectification which might have been activated over the voltage range studied (Stanfield, 1970). Fibers in solutions A and B from which capacitance data were obtained had resting potentials between −80 and −88 mV on initial electrode penetration, and the holding potential for each fiber was set at its initial resting potential. The solutions were cooled to 0.8-2.2°C.

In the first experiments fiber capacitance was measured as a function of membrane potential using test pulses of −8 to −10 mV applied 90–100 ms after the start of prepulses to different voltage levels. In order to improve signal/noise and thereby obtain accurate measurements of the small changes in capacitance observed in these solutions, from 10 to 40 sets of ΔV integrals were added on line and capacitance was calculated from the summed data. In accumulating summed data, a sequence using each of the selected levels of prepulse potential was repeated the desired number of times. This procedure tended to minimize the effect on the calculated voltage-dependent capacitance of any slow change of parameters such as r_i with time. Fig. 5 presents capacitance measurements made at four membrane potentials on each of nine fibers bathed in solution A. The data for each fiber have been normalized to the capacitance C_0 measured in that fiber at a membrane potential between −150 and −130 mV. At potentials of −115 to −100 mV the capacitance was essentially equal to that observed at the more negative membrane potentials, whereas depolarization to −75 to −55 mV caused a definite increase in capacitance in all fibers studied.

The relationship between fiber capacitance and membrane potential was seen more clearly by studying a given fiber over a range of membrane potentials. Fig. 6 presents relative fiber capacitance data determined from three sequences of measurements on one fiber using, successively, −10-, +10-, and −10-mV test pulses. Relative fiber capacitance is expressed as C/C_0, where C_0 for each sequence of measurements was the average of all capacitances measured at membrane potentials negative to −100 mV. The calculations were based on 10 summed sweeps at each level of voltage. In all cases the capacitance at membrane potentials negative to −100 mV was within 0.5% of C_0. With increasing depolarization from −100 mV, the capacitance increased monotonically. In order to avoid contraction the maximum value of V_2 was limited to −57 mV in this fiber.

Changes in effective fiber capacitance can be produced by changes in λ_T, the space constant of the T system. It is thus important to rule out the possibility that

the 15% increase in capacitance illustrated in Fig. 6 can be explained by an increase in λ_T, from a relatively low value at highly negative potentials to a near infinite value at the potential corresponding to the maximum measured capacitance. If surface capacitance is taken to be 1 μF/cm^2, independent of voltage,

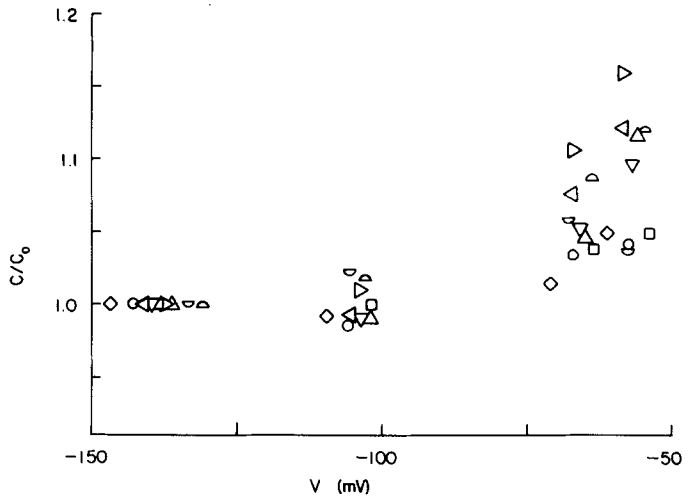

FIGURE 5. Variation of fiber capacitance with membrane potential in nine fibers in 5 mM Rb solution. Each symbol denotes data obtained from a given fiber. C_0 for each fiber was taken as the capacitance measured at a voltage between −130 and −150 mV. Each point represents the average capacitance calculated for pulse on and off using 15–40 summed sweeps. V is the membrane potential midway between $V_1(\infty)$ for the prepulse alone and $V_1(\infty)$ for the prepulse plus test pulse. The same convention applies to the abscissa in all subsequent graphs showing capacitance or conductance as a function of voltage. Holding potentials ranged from −80 to −86 mV. The time t_1 over which the capacitative transient was integrated was 7.5 ms for the fibers for which $\ell \simeq 185$ μm (△, ▽, and ▷) and 18 ms for the other fibers, $\ell \simeq 370$ μm. Values of C_0 (μF/cm^2) and fiber radius a (μm) for each fiber were 3.8 and 51 (○); 2.8, 35 (□); 7.0; 49 (◇); 4.2, 36 (△); 3.1, 35 (▽); 5.0, 49 (▷); 5.8; 44 (◁); 14.8, 63 (⌓); 8.3, 41 (⌔). No correction was made for leak conductances at the sites of electrode impalement in calculating the values of C_m given here and in all other figure legends. These data were obtained from fibers other than those in Table II. Solution A, 1.2 to 2.2°C.

tubular capacitance would need to increase from about 6 μF/cm^2 at $V < -120$ mV to about 7.1 μF/cm^2 at −64 mV. The ratio, 0.85, and the value 44 μm for fiber radius corresponds to $\lambda_T = 52$ μm (Eq. 14). Using a value greater than 1 μF/cm^2 for surface capacitance, which may be more appropriate for the end of a muscle fiber (Chandler and Schneider, 1976), would result in a smaller λ_T value.

Since the T-system conductance G_T must be less than the total fiber conductance G_m, the equation for G_T (Adrian et al., 1969, Equation 12) can be rearranged to give

$$\bar{G}_L = G_T \lambda_T I_0(a/\lambda_T)/I_1(a/\lambda_T) \tag{25}$$

$$\leq G_m \lambda_T I_0(a/\lambda_T)/I_1(a/\lambda_T). \quad (26)$$

Using the inequality with the maximum G_m of 3.8×10^{-4} mho/cm^2 measured at negative potentials in this fiber and the maximum λ_T value calculated above, $\bar{G}_L \leq 5$ μmho/cm. This corresponds to the low extreme of reported $\bar{G}_L$ values (Schneider, 1970; Hodgkin and Nakajima, 1972 *b*; Valdiosera et al., 1974 *b*; Chandler and Schneider, 1976). However, since fibers in solution B are predominantly permeable to Cl and since chloride conductance appears to be localized

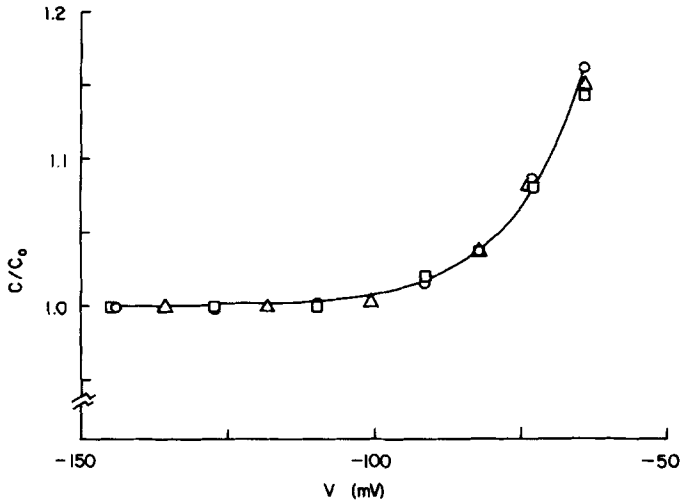

FIGURE 6. Effect of membrane potential on capacitance in 5 mM Rb solution. Different symbols represent results of three separate sequences of measurements on the same fiber: ○, first sequence, using a test pulse of −10 mV; △, second sequence, +10-mV test pulse; □, third sequence, −10-mV test pulse. Each point represents the average of on and off values calculated from 10 summed sweeps. C_0 for each sequence was taken as the mean of all capacitances measured at $V < -100$ mV in that sequence. The curve follows Eq. 27 with $V_{1/10} = -70$ mV, $k = 12.5$ mV. Fiber 101.2 (voltage traces obtained from this fiber are shown in Fig. 3). $V_H = -87$ mV, $\ell = 372$ μm, $\ell' = 28$ μm, $t_1 = 18$ ms. C_0 was 7.3, 7.0, and 6.9 μF/cm^2 in the first through third sequences, respectively, and a was calculated as 44 μm in each sequence. Solution B, 1.7°C.

in the surface membrane (Hodgkin and Horowicz, 1960; Eisenberg and Gage, 1969) G_T should be considerably smaller than G_m. In this case the $\bar{G}_L$ value necessary to explain the capacitance change on the basis of changing λ_T would be several times smaller than 5 μmho/cm, entirely too small to be consistent with reported values. The same argument can be applied to fibers in solution F, where G_m is much lower than in solution A or B but where similar changes in C/C_0 were observed.

When relatively large negative prepulses were used in 5 mM Rb solutions, ΔV slowly became less negative with time before the test pulse and after both the on and off test pulse capacitative transients. This apparently linear decrease of inward membrane current with time may be due to the slow exponential inactivation of chloride conductance

seen during large hyperpolarizations (Warner, 1972). It resulted in errors of opposite sign in both the conductances and in the capacitances calculated for pulse on and off. Thus, since all conductance and capacitance results presented here are averages of the values calculated for test pulse on and off at a given prepulse level, errors due to the slow ΔV component tended to cancel.

The correction procedure described in relation to the results in 100 mM K solution was, however, also used to subtract the contribution of the slow ΔV component from each measured ΔV integral. Comparing results based on corrected and on uncorrected ΔV data, it was decided to calculate fiber capacitances in 5 mM Rb solutions using the uncorrected data because of the following considerations: (*a*) Essentially the same voltage-dependent change in relative fiber capacitance was observed using corrected or uncorrected data, providing capacitances calculated for pulse on and off were averaged. (*b*) Using only measurements made at potentials positive to −120 mV, a voltage range over which the slowly changing ΔV component was negligible, the same voltage dependence of C/C_0 was observed as when the entire voltage range was studied. (*c*) The correction procedure, when used on all data presented in Fig. 5, appeared to introduce greater scatter into the results without changing the average voltage dependence of C/C_0.

A normalized measure of the voltage-dependent component of fiber capacitance is given by $(C - C_0)/C_0$. In each of six fibers studied at several voltages as in Fig. 6 $(C - C_0)/C_0$ increased exponentially with increasing V over the range studied, and could be conveniently described using the two-parameter empirical equation

$$\frac{C - C_0}{C_0} = \frac{\exp[(V - V_{1/10})/k]}{10}. \tag{27}$$

$V_{1/10}$ is the membrane potential at which the voltage-dependent capacitance component was 10% of the voltage-independent component and $1/k$ is a measure of the steepness of the exponential increase in capacitance with voltage. The curve in Fig. 6 is drawn according to Eq. 27 with $V_{1/10} = -70$ mV and $k = 12.5$ mV. These parameter values correspond to a line drawn by eye through a semilog plot of $(C - C_0)/C_0$ as a function of V for the fiber illustrated. Values of $V_{1/10}$ and k obtained for this and five other fibers in 5 mM Rb solution are listed in Table II. In solution B, the mean value of $V_{1/10}$ was −65 mV and the mean value of k was 12 mV.

VOLTAGE INDEPENDENCE OF r_i In capacitance measurements with the three-microelectrode technique the parameter actually measured is the product $r_i c_{\text{eff}}$. The capacitance data presented above were all calculated from $r_i c_{\text{eff}}$ measurements assuming r_i to be independent of voltage. However, since the voltage dependence of $r_i c_{\text{eff}}$ could also have resulted from a constant c_{eff} and a voltage-dependent r_i it was necessary to investigate the voltage dependence of r_i independently of c_{eff}. The approach used was outlined in the Theory section.

For r_i measurements, test pulses ranging from about +35 to −80 mV at the V_2 electrode were applied from a holding potential of −90 mV. No prepulses were employed. Since only steady-state values of voltages or current were relevant to the r_i analysis, each signal was monitored over two or three intervals before the pulse, during the pulse but after the decay of the on transient, and after the pulse after the decay of the off transient. During a

first sequence of pulses, ΔV and I were alternately monitored during each sweep. Next the sequence was repeated with V_2 monitored. Finally, the sequence was repeated once more, again monitoring ΔV and I. The two sets of ΔV and I data for each fiber were used independently for r_i analyses, with each analysis employing the same V_2 data. The results of the two r_i analyses for each fiber were then averaged. Effects of drift with time in the recording system or preparation were minimized by bracketing several pulses with repeat pulses of about +10 mV. Calculated values of $\bar{r}_i$ were expressed relative to the values of $\bar{r}_i$ calculated for the bracketing +10-mV pulses, with any change in the bracketing values distributed among the intervening pulses by assuming a linear drift in the +10-mV $\bar{r}_i$ value with time.

TABLE II

CHARACTERISTICS OF THE VOLTAGE-DEPENDENT COMPONENT OF FIBER CAPACITANCE IN ISOTONIC 5 mM Rb SOLUTIONS

Fiber	Solution	T	$V_{1/10}$	k	$\tilde{V}$*
		°C	mV	mV	mV
97.6	A	2.2	−58	16	−14
101.2	B	1.7	−70	12	−34
101.4	B	0.8	−68	12	−32
101.5	B	2.0	−62	10	−30
102.3	B	1.7	−64	15	−22
102.4	B	1.5	−62	10	−30
Mean ± SEM‡			−65±2	12±1	−30±2

* In calculating $\tilde{V}$ by Eq. 32, Q_{MAX}/C_0 was assumed to equal 24.5 nC/μF, the mean value determined by Chandler et al. (1976 *a*) in fibers in a sucrose hypertonic solution having the same ionic composition as solution B. Values of δ varied from 4.4 to 4.7 mV.

‡ Only the five fibers studied in solution B were used for calculating mean parameter values.

Fig. 7 presents $\bar{r}_i$ values as a function of V calculated according to Eq. 24 for each of four fibers. For comparison with Figs. 5 and 6, the ordinate employed is $\bar{r}_i/\bar{r}_0$, where $\bar{r}_0$ is the average of the $\bar{r}_i$ values determined at membrane potentials negative to −100 mV. For $F\{V\} = 1$ (open and half-filled symbols) $\bar{r}_i/\bar{r}_0$ was close to unity at all membrane potentials. The experimental measurements are thus consistent with $F\{V\} = 1$ and, consequently, with the hypothesis that r_i is independent of membrane potential.

An alternative hypothesis, namely that r_i varies with membrane potential in such a way as to account for the average measured voltage dependence of $r_i c_{eff}$, corresponds to the filled and half-filled symbols in Fig. 7. Here mean values from Table II were used with Eq. 27 to give 0.1 exp [$(V + 52)/12.5$] as the trial function for $F\{V\}$. Since these experiments were carried out in solution A whereas the mean values in Table II apply to solution B, $V_{1/10}$ was taken as −52 rather then −65 mV. This change in $V_{1/10}$ was assumed because charge movement experiments in solutions A and B made hypertonic by sucrose addition showed that replacing Na with TEA caused a negative shift of 13 mV of the charge versus voltage curve along the voltage axis (Chandler et al., 1976 *b*). The

fact that the filled symbols deviate increasingly from unity for V increasingly positive to −100 mV shows that this $F\{V\}$ trial function is not consistent with the experimental observations. Thus the $r_i c_{eff}$ voltage dependence cannot all be accounted for by a voltage-dependent change in r_i. Although it is conceivable that both r_i and c_{eff} depend on voltage, it seems simplest to conclude that only c_{eff} varies with voltage and that r_i is constant.

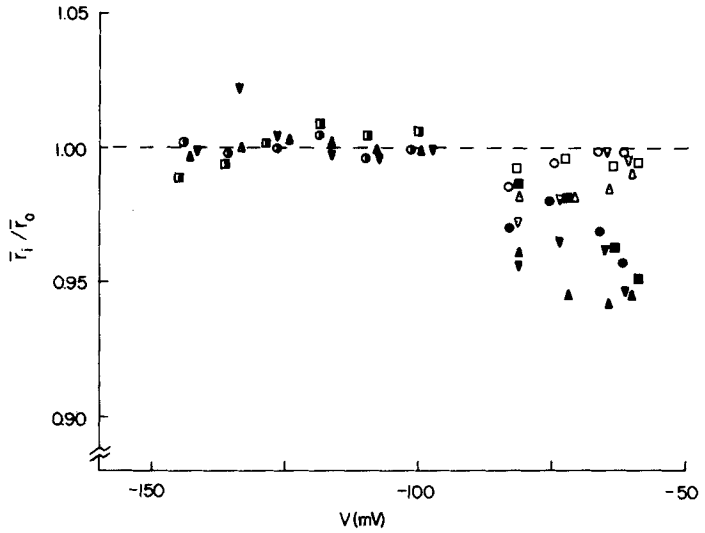

FIGURE 7. Test of two hypotheses regarding the effect of membrane potential on r_i. $\bar{r}_i$ values were calculated according to Eq. 24 for each of two trial functions $F\{V\}$ and were normalized by $\bar{r}_o$, the mean of the $\bar{r}_i$ values for $V < -100$ mV. An $\bar{r}_i/\bar{r}_o$ value of 1.0 signifies agreement of $F\{V\}$ with the experimental measurements. Open symbols correspond to $F\{V\} = 1$, i.e. r_i independent of V. Filled symbols correspond to $F\{V\} = 0.1 \exp[(V + 52)/12.5]$. Half-filled symbols indicated superimposed open and filled symbols. Each symbol gives results from a different fiber. $\ell \simeq 740$ μm, $-92 \leq V_H \leq -90$ mV. The $\bar{r}_o$ values (megohms per centimeter) for these fibers were 4.71 (◑), 4.85 (◨), 3.95 (▲), and 3.86 (▼). *R. pipiens*, solution A, 19–21°C.

The experiments illustrated in Fig. 7 were carried out on sartorius muscles from *R. pipiens*. However, since both *R. pipiens* and *R. temporaria* exhibited similar voltage-dependent changes in $r_i c_{eff}$ it seems safe to conclude that c_{eff} rather than r_i is the voltage-dependent element in both species.

A possible source of error in the $\bar{r}_i$ analysis is that all calculations were carried out assuming infinite leak resistances at the sites of electrode impalement. To account for the effects of r_1, the leak resistance at the V_1 electrode, and of r_2, the effective parallel resistance of the leaks at the V_2 and I electrodes, a modified $\bar{r}_i$ analysis was carried out using Eqs. 2*a*, 6*a*, 9*a*, 13*a*, and 14*a*. Values of r_1 and r_2 were estimated from fiber input resistance and the small depolarizations which occurred when the microelectrodes V_1 and I were initially inserted. The results of the analysis were essentially the same as the results obtained assuming infinite leak resistances.

RELATIONSHIP BETWEEN VOLTAGE-DEPENDENT CAPACITANCE AND MEMBRANE CHARGE MOVEMENT The observed increase in fiber capacitance with increasing

depolarization from −100 mV to below the contraction threshold can be explained on the basis of voltage-dependent redistribution of charged particles in the fiber membrane (Schneider and Chandler, 1973). Movement of these particles on depolarization, and their return on repolarization, will contribute an extra component of capacitative charging current. Considering the membrane to be composed of two capacitative elements, an ideal voltage-independent capacitance C_0 and a population of mobile charged particles which can move between different locations within the membrane, the membrane capacitance for infinitely small displacements in V would equal $C_0 + dQ/dV$. Q is the amount of extra charge in the external circuit which is required to offset the effects of the mobile charge which has migrated at voltage V.

In practice capacitance is measured as the change in charge for a step change in membrane potential from V_α to V_β, so that its value, assigned to the potential midway between V_α and V_β, would be

$$C = C_0 + \frac{Q_\beta - Q_\alpha}{V_\beta - V_\alpha}. \tag{28}$$

Q_α and Q_β are the values of Q at the respective membrane potentials V_α and V_β. The convention used is that at large negative values of membrane potential, Q is set equal to zero. The equation relating Q to V used by Schneider and Chandler (1973),

$$Q = \frac{Q_{MAX}}{1 + \exp[-(V - \bar{V})/k]}, \tag{29}$$

is determined by three parameters: Q_{MAX}, the maximum amount of Q; $\bar{V}$, the membrane potential at which half the charge has migrated in the steady state; and k, a measure of the steepness of the variation of Q with V.

Eqs. 28 and 29 can be combined to give

$$\frac{C - C_0}{C_0} = \frac{Q_{MAX}}{2\delta C_0}\left[1 + \exp - \left(\frac{V + \delta - \bar{V}}{k}\right)\right] \left[1 + \exp - \left(\frac{V - \delta - \bar{V}}{k}\right)\right], \tag{30}$$

where δ is equal to $(V_\beta - V_\alpha)/2$. For large negative values of $(V - \bar{V} + \delta)/k$ Eq. 30 can be simplified to

$$\frac{C - C_0}{C_0} = \left[\frac{Q_{MAX}\exp(-\bar{V}/k)}{\delta C_0}\sinh(\delta/k)\right]\exp(V/k) \tag{31}$$

For the experimental measurements constant voltage steps were applied from different holding potentials, so that δ would be constant and the extra capacitance should increase exponentially with voltage. Since the right-hand sides of Eqs. 31 and 27 are both of the form $A \exp(V/k)$, A being a constant, the values of k in the two equations must be equal. The mean value of k measured in solution B was 12 mV (Table II). This value is in agreement with the values 11 mV (Schneider and Chandler, 1973) and 8 mV (Chandler et al., 1976 *a*) calculated

from measurements of extra charge movement over a large range of membrane potentials in fibers in hypertonic solutions (solution B plus 467 mM sucrose) at 0–2°C. Assuming a Boltzmann distribution of mobile charged particles between two membrane locations which differ in potential by the entire value of V, k is equal to $|RT/zF|$ (Schneider and Chandler, 1973), where z is the particle valence, R is the gas constant, T is absolute temperature, and F is the Faraday constant. The mean value of k in Table II thus corresponds to a particle valence of 2.

Since the constant multiplying $\exp(V/k)$ in Eq. 31 is a function of both $\bar{V}$ and Q_{MAX}, these two parameters cannot be determined from capacitance data obtained over the voltage range of applicability of Eq. 31. Estimates of $\bar{V}$ can be obtained, however, by assuming that Q_{MAX}/C_0 is the same in isotonic and sucrose hypertonic solutions. Setting Eqs. 27 and 31 equal and rearranging, one obtains

$$\bar{V} = V_{1/10} + k \ln \left[\frac{10\ Q_{MAX} \sinh(\delta/k)}{\delta C_0} \right]. \tag{32}$$

The values of $\bar{V}$ obtained using measured $V_{1/10}$ and k values and the mean value, 24.5 nC/μF, of Q_{MAX}/C_0 measured in sucrose hypertonic solution B (Chandler et al., 1976 *a*) gave a mean $\bar{V}$ of −30 mV (Table II).

Muscles Bathed in 100 mM Rb Solution

VOLTAGE-DEPENDENT CAPACITANCE IN DEPOLARIZED FIBERS. The voltage dependence of membrane in capacitance in depolarized fibers was studied using a 100 mM Rb, Cl-free SO_4 solution (solution C, Table I). In this solution fiber membrane conductances are low and relatively independent of voltage so that conductance-dependent changes in apparent fiber capacitance should be minimal. The resting potentials of the fibers studied in this solution ranged from −29 to −31 mV (17.5 to 18.6°C) and the holding potential for each fiber was set equal to its membrane potential.

In both the 100 mM Rb and 100 mM K solutions, as in the 5 mM Rb solution, capacitance and conductance were measured using small constant test pulses of about +10 or −10 mV superimposed on variable-sized prepulses. The averaging procedures used in the experiments in 5 mM Rb were not used in these experiments. Rather, in order to carefully measure relative changes in capacitance and to avoid problems of drift, each capacitance measurement using a prepulse was preceded and followed by a measurement from the holding potential. Relative capacitances were calculated as the ratio of capacitances measured with a prepulse to the mean of the bracketing capacitances measured using no prepulse. Relative capacitances measured using −10- and +10-mV test pulses were made comparable by scaling the latter by the average ratio of control capacitances for −10- and +10-mV pulses obtained during the course of each experiment.

Fig. 8 presents capacitances measured in one fiber over an approximately 200-mV range of potentials and normalized to C_0, the assumed voltage-independent capacitance. The C/C_0 value of 1.09 at −33 mV, indicated by the filled circle, corresponds to a −10-mV pulse applied from the holding potential. As V was made more positive, C/C_0 decreased. In the neighborhood of +35 to +65 mV C/C_0 seemed to approach a relatively constant value. This is not apparent in Fig.

8 because of the scatter in the points, and the beginning of a second phase of decreasing capacitance, but is seen if average data from several fibers are used (Fig. 9). At membrane potentials positive to +65 mV the fiber in Fig. 8 exhibited a fall in capacitance. When V was made more negative than −33 mV, C/C_0 increased and reached a maximum of about 1.19 in the neighborhood of −80 to −90 mV (Fig. 8). With further hyperpolarization, C/C_0 appeared to decline.

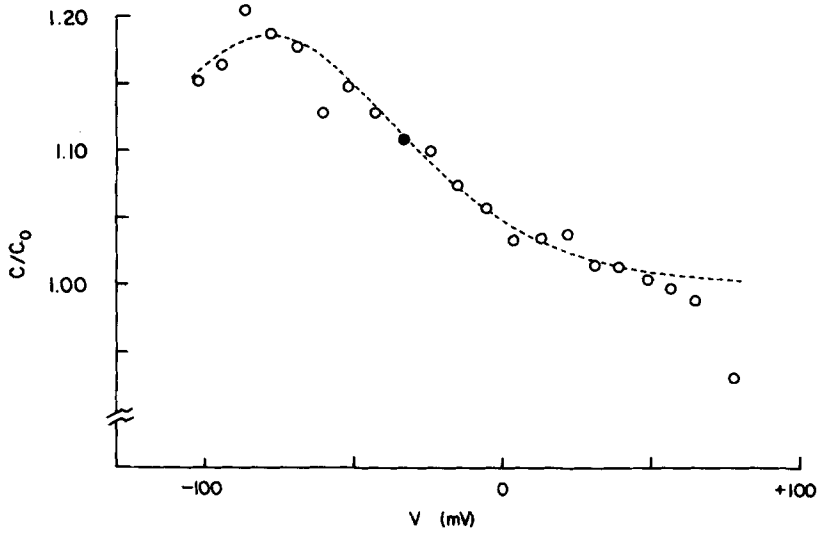

FIGURE 8. Variation of capacitance with membrane potential in a fiber in 100 mM Rb solution. Each point gives the average of four C/C_0 values, the on and off values of two determinations using either +10- or −10-mV test pulses. These capacitances, as well as those in Figs. 9–11, were initially measured relative to C_{ref}, the value determined using a −10-mV pulse applied from the holding potential. The value 1.09 of C_{ref}/C_0 (filled circle) used to normalize capacitance to C_0 was obtained by rearranging Eq. 30 and fitting it to the C/C_{ref} data for $V < 50$ mV, excluding the point at −61 mV. The theoretical curve corresponds to Eq. 30 with $k = 30.1$ mV, $Q_{MAX}/C_0 = 22.4$ nC/μF, and $\bar{V} = -79$ mV, the other parameter values determined by the curve-fitting procedure. $V_H = -29$ mV, $\ell = 736$ μm, $\ell' = 18$ μm, $t_1 = 36$ ms, $C_0 = 8.1$ μF/cm^2, and $a = 43$ μm. Solution C, 18.0°C.

The capacitance change in Fig. 8 for $V < 50$ mV cannot be accounted for on the basis of a change in λ_T. c_{eff} changed from 8.3 to 9.6 μF/cm^2 in going from +30 to −80 mV. Assuming a surface capacitance of 1 μF/cm^2 and that the observed change in capacitance was due to a fall in a/λ_T from a relatively high value to zero, the value of a/λ_T at +30 mV which satisfies Eq. 14 is 0.81. At +30 mV, G_m in this fiber was less than 0.12 mmho/cm^2. Using these values for G_m and a/λ_T and the calculated radius of 43 μm, the upper bound on $\bar{G}_L$, calculated according to Eq. 26, is 1.7 μmho/cm. If the T system contributed only a fraction of the fiber conductance at +30 mV, the maximum $\bar{G}_L$ value would be proportionately reduced. The necessity of invoking such a low $\bar{G}_L$ value and the fact that G_m is about twice as high at −80 as at +30 mV make it unlikely this capacitance change in 100 mM Rb solution was due to conductance changes in the T system.

A similar analysis of the increase in c_{eff} from 7.5 to 8.1 μF/cm^2 on going from +77 to +50 mV, which was accompanied by a fall in G_m from 1.1 to 0.2 mmho/cm^2, gives $\bar{G}_L < 28$ μmho/cm, a reasonable upper bound. Thus the fall in capacitance at $V > 50$ mV in Fig. 8 may be attributable to a fall in λ_T due to increasing G_T. This effect will not be considered further.

The curve in Fig. 8 gives the relationship between C/C_0 and V as predicted by the two-position mobile charge movement model, Eq. 30. The fitted parameters were $\bar{V} = -79$ mV, $k = 30.1$ mV, and $Q_{MAX}/C_0 = 22.4$ nC/μF. These numbers should be considered as only approximate since the data are somewhat scattered and do not adequately describe the range $V < \bar{V}$.

Average values of C/C_0 for five fibers in 100 mM Rb solution are plotted as a function of V in Fig. 9. In agreement with results from the single fiber in Fig. 8,

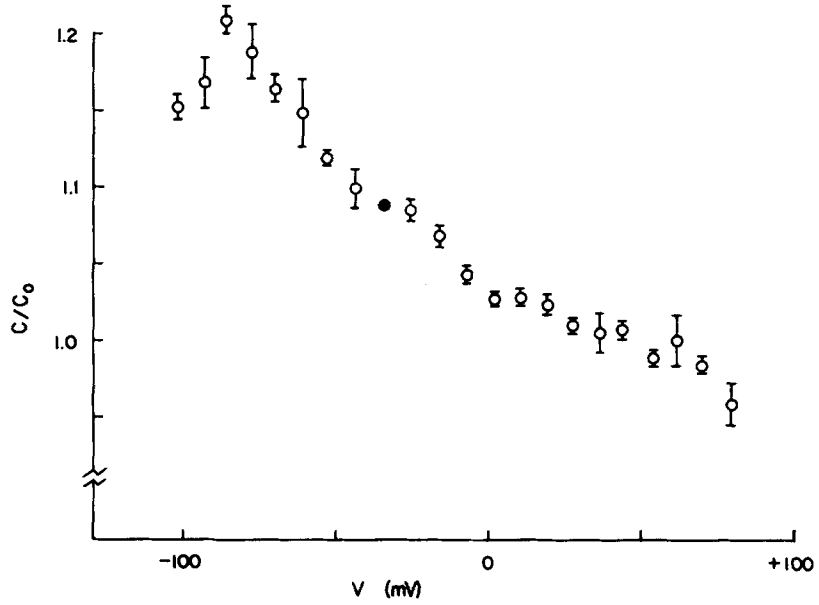

FIGURE 9. Mean variation fiber capacitance with membrane potential in five fibers bathed in 100 mM Rb solution. Each point was obtained by multiplying the mean value of C/C_{ref} at a given V by C_{ref}/C_0, determined as the average of four C/C_{ref} values for $35 < V < 65$ mV. The filled circle without error bars indicates C_{ref}/C_0. Error bars give ±1 SEM. Here and in Fig. 10, ±1 SEM about the mean voltage for each point was smaller than the size of the symbols. $\ell \simeq 740$ μm, $t_1 = 36$ ms and $-31 \leq V_H \leq -29$ mV. The fibers had the following values for C_0 and a (μF/cm^2 and μm): 8.1 and 43 (same fiber as in Fig. 8); 9.2, 45; 6.4, 32; 6.5, 42; 11.1, 60. Solution C, 17–19°C.

the average capacitance increased gradually as V was made increasingly negative with respect to +50 mV, reaching a peak at a membrane potential between about −80 and −90 mV. The least squares parameter values for the average capacitance data were $\bar{V} = -86.5$ mV, $k = 30.2$ mV, and $Q_{MAX}/C_0 = 22.4$ nC/μF, in agreement with those for the fiber in Fig. 8.

Despite the degree of uncertainty in parameter values, it is clear that this voltage-dependent capacitance differs from that observed in polarized fibers in solutions A and B. At 18°C its $\tilde{V}$ value is about 50–60 mV more negative than $\tilde{V}$ in solution B at 2°C and its k value is about 2.5 times larger than k in solutions A and B at 2°C (Table II). The values of Q_{MAX}/C_0 for the two capacitances appear, however, to be about the same.

Muscles Bathed in 100 mM K Solution

The 100 mM K, Cl-free SO_4 solution (solution D, Table I) was identical with the 100 mM Rb solution except that K was used in place of Rb. The range of membrane and holding potentials of fibers in this solution was −13 to −17 mV (16.7 to 18.4°C).

The data acquisition routine used to study capacitance and conductance was the same as that used for fibers in 100 mM Rb solution with one exception. Because of slow changes in K conductance which are seen at large hyperpolarizations (Adrian and Freygang, 1962; Adrian et al., 1970 *b*; Almers, 1972 *a*), the ΔV integrals were corrected for slowly changing ionic components by subtracting sloping base lines.

The slow ΔV component was assumed to vary linearly with time but at different rates before, during, and after the test pulse. During or after a test pulse it was assumed to begin, respectively, at the on or the off of the test pulse. Assuming the capacitative current to be negligible by the end of the third interval after pulse on or off, the rate of change of the linear ΔV component was assumed to correspond to the average rate of change during the next four ΔV integrals. The rate of change of the linear ΔV component before the test pulse was assumed to correspond to the average rate of change of the three ΔV integrals measured before pulse on.

VOLTAGE-DEPENDENT CAPACITANCE DUE TO CHARGE MOVEMENT The variation of fiber capacitance over the voltage range $+15 < V < +65$ mV for fibers in either 100 mM K solution (circles) or 100 mM Rb solution (squares) is illustrated in Fig. 10. Here the capacitance values for each fiber are expressed relative to the mean capacitance C_{mean} calculated for that fiber from six measurements within the specified V range. The average values of C/C_{mean}, plotted in Fig. 10, exhibited about the same variation with V in the two solutions. Consequently, the charge movement process responsible for the capacitance changes observed in 100 mM Rb appears also to be present in the 100 mM K solution.

CONDUCTANCE-DEPENDENT CHANGES IN FIBER APPARENT CAPACITANCE In addition to the variation in capacitance observed in both 100 mM Rb and 100 mM K solutions and attributed to a charge movement process, fibers in 100 mM K solution also exhibit a second, more pronounced change in capacitance. This second type of change is accompanied by a large inwardly rectifying component of membrane conductance (Katz, 1949) which is not present in the 100 mM Rb solution (Adrian, 1964).

The circles in Fig. 11 A show values of G_m as a function of membrane potential from a fiber in 100 mM K solution. Since the raw data for the calculations were provided by test pulses of ±10 mV superimposed on prepulses to various levels

of potential, G_m approximates the fiber slope conductance. The filled circle in Fig. 11 A indicates the value of G_m measured using a −10-mV test pulse applied from V_H. G_m clearly decreased when V was made more positive and increased when V was made more negative. For the largest voltage displacements employed, both positive and negative, G_m became independent of V.

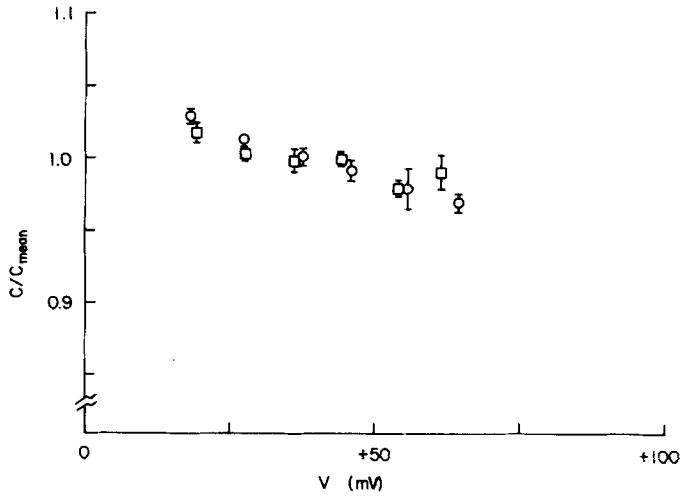

FIGURE 10. Voltage dependence of capacitance over a positive range of membrane potentials for fibers in 100 mM K or 100 mM Rb solutions. Squares give average results from five fibers in Rb solution (solution C) and circles give averages from four fibers in K solution (solution D). Error bars give ±1 SEM. For each fiber, capacitance was normalized to the mean value C_{mean} measured at the six voltages. The five fibers in Rb solution are the same as in Fig. 9 and had C_{mean} values of 8.2, 9.3, 6.4, 6.5, and 11.0 μF/cm^2 (listed in the same sequence for Fig. 9). For the fibers in K solution $\ell \simeq 370$ μm, $t_1 = 12$ ms, and $-16 \leq V_H \leq -13$ mV (18°C). They had the following C_{mean} and a values (μF/cm^2 and μm): 10.4 and 86; 9.0, 74; 7.0, 38; 8.4, 46.

For the sake of comparison, the squares in Fig. 11 A give the mean values of G_m measured in five fibers in 100 mM Rb solution. In the Rb solution, G_m was small and essentially independent of V. The lowest values of G_m measured in 100 mM K solution at strongly positive voltages correspond to the G_m values of fibers in 100 mM Rb solution. It would thus be reasonable to try to relate any capacitance increase which occurred from −50 to 0 mV in K solution to the relatively large voltage-dependent component of G_m.

Fig. 11 B presents C/C_0 data in 100 mM K solution from the same experiment as Fig. 11 A. The filled circle, $C/C_0 = 0.867$, corresponds to the −10-mV test pulse applied from the holding potential. This locates the reference voltage V_{ref}. For voltages slightly positive to V_{ref}, the capacitance increased steeply with increasing V. At more positive V, C/C_0 reached a maximum and then declined gradually as V increased further. The latter effect is attributed to the properties of the charge movement system studied using 100 mM Rb solution and discussed

in the preceding section. Over the voltage range slightly negative to V_{ref}, C/C_0 first decreased steeply and then increased with decreasing V. At the most negative V values used, roughly −55 to −65 mV, C/C_0 appears to be relatively independent of V. The 2% change in C/C_0 between −55 and −65 mV observed in the 100 mM Rb solution (Fig. 9) could also be present in the 100 mM K solution but be obscured by the scatter in the data. Patterns of C/C_0 variation with V similar to that in Fig. 11 B were observed in the three other fibers which were studied in the same manner.

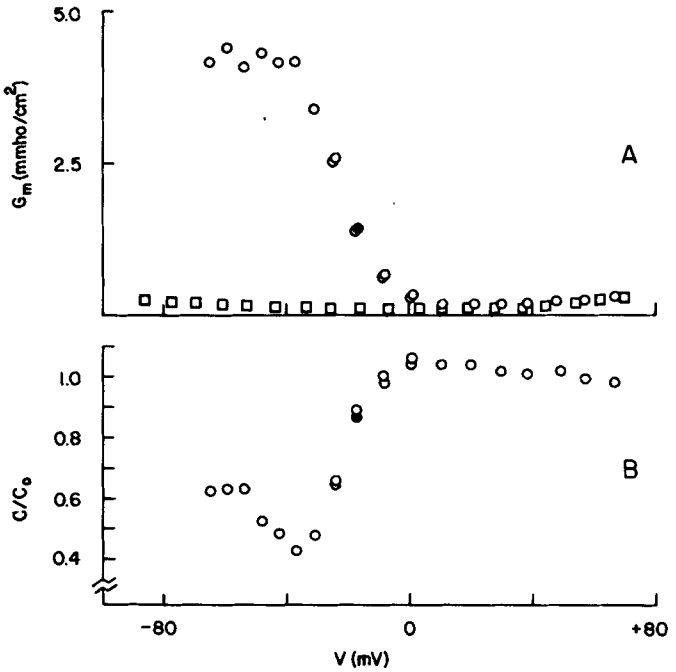

FIGURE 11. Effect of membrane potential on conductance and capacitance of a fiber in 100 mM K solution. (A) Circles give values of G_m measured in a fiber in solution D using ±10-mV test pulses. The filled circle gives G_m for the negative test pulse applied from V_H. Each circle in parts A and B represents the mean of two determinations using the same pulse sequence. The squares in A give mean G_m values calculated for five fibers in 100 mM Rb solution, same fibers as illustrated in Fig. 9. ±1 SEM for each square is smaller than its size. The horizontal axis is the same for A and B. (B) Same fiber as in A. Each point gives C/C_0 calculated as for Fig. 9, except that data from only one fiber were used. All values of capacitance were calculated after applying a linear correction for ionic currents (see text). The filled circle indicates $C_{ref}/C_0 = 0.867$. The mean capacitance C_0 for $+35 < V_m < +65$ mV was 8.1 μF/cm^2. $\ell = 376$ μm, $t_1 = 12$ ms, $V_H = -13$ mV, and $a = 46$ μm (18.6°C).

The steep increase of C/C_0 at V levels slightly positive to V_{ref} can be explained on the basis of potential-dependent changes in λ_T. At V_{ref} the fiber K conductance is roughly one-third its maximal value (filled circle, Fig. 11 A). Since as much as three-fourths of this inwardly rectifying K conductance may be located in the T system (Almers, 1972 *b*), a/λ_T would be expected to be significantly

greater than zero at V_{ref}. Under these conditions, $c_T(a/\lambda_T)$ would be less than the total T-system capacitance $c_T(0)$ (Eq. 14). For membrane potentials slightly positive to V_{ref}, the decrease in G_m (Fig. 11 A) would bring a/λ_T close to zero, and $c_T(a/\lambda_T)$ would approach $c_T(0)$, thus giving the observed increase in total measured capacitance.

The fact that C/C_0 is relatively small and constant for potentials between −55 and −65 mV can also be explained on the basis of changes in λ_T. Over this voltage range G_m is constant and about three times larger than at V_{ref} (Fig. 11) so that a/λ_T would be larger and $c_T(a/\lambda_T)$ smaller than at V_{ref}.

The observed minimum in C/C_0 at voltages slightly negative to V_{ref} appears to be inconsistent with the observed monotonic increase in G_m as V is made negative to V_{ref}. However, it should be noted that the capacitance analysis relies on linear cable theory and is therefore valid only if G_m is constant. For example, if g_m in Fig. 2 changes during a pulse, the ionic current at the V_1 electrode is no longer proportional to $V_1\Delta V(\infty)/V_1(\infty)$, and Eq. 6 is no longer valid. Since membrane conductance is strongly voltage dependent at voltages near V_{ref} (Fig. 11 A), errors in capacitance measurements may have occurred in this voltage range. Any time dependence in the inward rectifier conductance change would further complicate the analysis. For $-40 < V < -10$ the capacitance calculated for the negative transient of either a −10- or a +10-mV pulse was consistently smaller than that calculated for the positive transient of the same pulse. No such nonlinearity was detected at voltages further from V_{ref}, where capacitances calculated for pulse on and off did not differ systematically and were in most cases essentially the same.

In the following analysis only capacitance values for relatively large displacements from V_{ref} were used for estimating a/λ_T. The analysis relies on the assumption that for these voltages the change in inward rectifier conductance was the sole cause of the observed changes in capacitance.

DETERMINATION OF THE T-SYSTEM SPACE CONSTANT A second series of experiments in 100 mM K solution was designed to compare fiber capacitances under the conditions of either maximal or minimal activation of inward rectification and to separate surface and T-system components using an analysis of the time-course of ΔV. Test pulses of ±10 mV were superimposed on either a large negative or large positive prepulse, the sequence being repeated for a total of 10 times. The summed ΔV integrals were analyzed in the usual way whereas the time-course was analyzed from pointwise sampling using conventional analog-to-digital conversion (Chandler and Schneider, 1976).

The results of the experiments are listed in Table III. Column 1 gives the fiber reference and column 2 gives the voltage during the prepulse. The values of $r_i c_{eff}$ in column 3 were obtained from analyzing only the on ΔV integrals since the time-course was measured only during the on. Each value in columns 3 and 4 represents the average obtained with a +10- and a −10-mV test pulse. The surface membrane contribution $r_i c_m'$ to $r_i c_{eff}$, as determined for each fiber from analysis of ΔV time-course at the positive voltage level (Chandler and Schneider, 1976), is given in column 4. Assuming the surface membrane capacitance to be

independent of voltage, this $r_i c_m'$ value can be subtracted from both the positive and negative prepulse values of $r_i c_{eff}$ to give the T-system contribution $r_i c_T$ at each of the two voltages, column 5. Assuming λ_T to be infinite at the positive voltage, the ratio of $r_i c_T$ values gives $c_T(a/\lambda_T)/c_T(0)$, column 6. The a/λ_T values corresponding to each $c_T(a/\lambda_T)/c_T(0)$ value, calculated according to Eq. 14, are listed in column 7. Over the voltage range of −59 to −66 mV, where inward

TABLE III

ESTIMATE OF T-SYSTEM SPACE CONSTANT FROM CAPACITANCE CHANGE WITH INWARD RECTIFICATION IN 100 mM K SOLUTION

1 Fiber	2 Prepulse voltage	3 $r_i c_{eff}$	4* $r_i c_m'$	5 $r_i c_T$	6‡ $c_T(a/\lambda_T)/c_T(0)$	7‡ a/λ_T	8‡ λ_T
	mV	*ms/cm²*	*ms/cm²*	*ms/cm²*			*μm*
91.1	44	687	307	380	0.761	1.12	48.6
	−66	596	(307)	289			
92.1	43	636	138	498	0.761	1.12	33.2
	−62	517	(138)	379			
92.2	45	709	128	581	0.448	2.31	20.4
	−59	388	(128)	260			
93.1	44	600	205	395	0.643	1.51	27.1
	−63	459	(205)	254			
93.2	40	657	40	617	0.645	1.50	22.5
	−60	438	(40)	398			
94.2	44	696	154	542	0.712	1.28	37.2
	−64	540	(154)	386			
Mean ± SEM							31.5 ±4.3

* Positive prepulse values of $r_i c_m'$ were determined from an analysis of the time-course of ΔV (Chandler and Schneider, 1976); negative and positive prepulse values were assumed to be equal.
‡ λ_T was assumed to be infinite and therefore a/λ_T to be zero at positive prepulse voltages.
l = 172–190 μm, 16.7 – 18.4°C. See text for details of calculations.

rectification is fully activated (Fig. 11 A), λ_T was roughly three-fourths the fiber radius. Using the radius calculated for each fiber, λ_T was found to range from 20.4 to 48.6 μm (column 8), with a mean value of 31.5 μm. The mean λ_T value determined in four other experiments, using wider electrode spacing similar to the experiment in Fig. 11, was 23.8 μm; for these calculations the surface capacitance was assumed to be 2.0 μF/cm² (Chandler and Schneider, 1976).

If the voltage-dependent component of fiber capacitance seen in 100 mM Rb solution and attributed to nonlinear charge movement were also present in 100 mM K solution, as is indicated by Fig. 10, its effects on the λ_T analysis should be considered. In going from the average positive prepulse voltage of +43 mV to

the average negative voltage of −62 mV, fibers in 100 mM Rb solution exhibited a mean increase in capacitance of 11% when the Rb data were subjected to the same linear correction as was used in analyzing the results in 100 mM K solution. Assuming the charge responsible for this capacitance component to be uniformly distributed in the surface and T-system membranes and to be the same in Rb and K solution, the value of $r_i c_{\text{eff}}$ at the negative prepulse would include a component of about 11% due to charge movement. Correction for this effect caused the mean value of λ_T in Table III to decrease from 31.5 to 24.4 μm.

SURFACE AND TUBULAR LOCALIZATION OF INWARD RECTIFICATION The distribution of inward rectifier channels in the surface and tubular membranes is considered in Table IV, same fibers as Table III. Column 2 gives the difference in the $r_i g_m$ values measured at negative and positive voltages, $\Delta(r_i g_m)$; this is equal to the contribution of the fully activated inward rectifier system. Since the value is obtained as the difference between two values of $r_i g_m$, the errors introduced by an electrode leak at V_1 cancel (Appendix A).

TABLE IV

ESTIMATE OF FRACTION OF INWARD RECTIFIER CHANNELS LOCATED IN THE T SYSTEM

1 Fiber	2 $\Delta(r_i g_m)$	3 $r_i g_T(a/\lambda_T)$	4 $r_i g_m'$	5 $r_i g_T(0)$	6 $g_T(0)/[g_m' + g_T(0)]$	7 $c_T(0)/[c_m' + c_T(0)]$
	cm^{-2}	cm^{-2}	cm^{-2}	cm^{-2}		
91.1	302.4	143.7	158.7	167.9	0.514	0.553
92.1	483.0	288.5	194.5	336.9	0.634	0.783
92.2	636.0	658.7	−22.7*	1025.9	1*	0.819
93.1	304.6	218.5	86.1	274.3	0.761	0.658
93.2	340.9	293.4	47.5	367.6	0.886	0.939
94.2	353.5	210.7	142.8	250.1	0.637	0.779
Mean ± SEM					0.739 ± 0.074	0.755 ± 0.056

Column 2 gives the difference between negative and positive prepulse values of $r_i g_m$. Column 3 gives the negative prepulse value of $r_i g_T$ calculated using a/λ_T from Table III and values of $r_i \bar{G}_L$ obtained from analysis of the ΔV time-course (Chandler and Schneider, 1976). Column 4 gives the difference between columns 2 and 3. Column 5 gives the value of $r_i g_T$ which would have been observed if $\bar{G}_L$ had been infinite. Column 6 gives the fraction of inward rectifier channels in the T system and column 7 gives the fraction of membrane capacitance in the T system. Same fibers as in Table III. See text for details of calculation.

* For fiber 92.2, the calculated $r_i g_T$ value was greater than the total measured $\Delta(r_i g_m)$; in this case the fraction of inward rectifier channels in the T system, column 6, was set at unity.

Column 3 of Table IV gives the contribution of the T system to $\Delta(r_i g_m)$ when inward rectification is fully activated. This was calculated according to

$$r_i g_T(a/\lambda_T) = \frac{2\pi a r_i \bar{G}_L}{\lambda_T} \frac{I_1(a/\lambda_T)}{I_0(a/\lambda_T)} \tag{33}$$

(Adrian et al., 1969) using values of a/λ_T from Table III and values of $r_i\bar{G}_L$ from the ΔV time-course analysis (Chandler and Schneider, 1976). The contribution of the fully activated surface membrane, $r_i g_m'$ (column 4), is simply the difference between columns 2 and 3.

In order to compare the number of inward rectifier channels in the surface and T-system membranes it is necessary to make a small correction for the effect of the T-system luminal conductance $\bar{G}_L$, which is not infinite. Column 5 of Table IV gives the maximum contribution of the T system, $r_i g_T(0)$, that would in theory have been observed had $\bar{G}_L$ been infinite. This was calculated as $\pi r_i \bar{G}_L (a/\lambda_T)^2$ and is equal to $r_i \pi a^2 \bar{G}_W$, where $\bar{G}_W$ is the T-tubule membrane conductance per unit volume of muscle fiber. Column 6, $g_T(0)/(g_T(0) + g_m')$, gives what would have been the T-system fraction of fully activated inward rectifier conductance had $\bar{G}_L$ been infinite. This ratio, 0.74, equals the fraction of inward rectifier conductance channels located in the T system. For comparison, the fraction of fiber capacitance due to the T system when $a/\lambda_T = 0$, calculated using data from Table III, is given in column 7. These values are close to those in column 6, indicating that the density of inward rectifier channels is about the same in the surface and tubular membranes if the specific capacitances of the two membranes are the same. The fraction of inward rectifier channels calculated to be located in the T system is in agreement with the earlier estimates of 78% (Almers, 1972 *b*) and 66% (Eisenberg and Gage, 1969) of the fraction of K conductance contributed by the T system.

DISCUSSION

Three different effects of voltage on capacitance have been described for skeletal muscle fibers immersed in isosmotic solutions. The first effect concerns the monotonic increase in capacitance seen in normally polarized fibers when the potential is varied from about −100 mV to near the contraction threshold. The second effect is seen when the muscle is depolarized by a high Rb-containing solution. In this case the capacitance is also voltage dependent, but the relationship is different from that observed in polarized fibers. Both of these changes can be seen under conditions in which fiber conductance is very low and, consequently, λ_T is large.

The third effect of voltage on capacitance can be observed in fibers in a high potassium solution. Turning on inward rectification by hyperpolarization increases the conductance of the membranes of the T system. The associated decrease in λ_T produces a decrease in the measured capacitance. Each of these three effects will be discussed in the following sections.

Voltage-Dependent Capacitance in Normally Polarized Fibers

The properties of this process in many respects resemble the properties of the voltage-dependent charge movement which has been observed in fibers in which contraction was blocked by hypertonicity (Schneider and Chandler, 1973; Chandler et al., 1976 *a*). The charge movement experiments are best explained by assuming that there are mobile charges or dipoles confined to the membrane which can change their distribution in reponse to changes in membrane poten-

tial. The redistribution associated with depolarization contributes an outward current and the return on repolarization contributes an inward current. These time-dependent currents are characterized by the fact that equal charge is carried by each transient. Since the amount of charge which moves is a nonlinear function of V, the process would be expected to give rise to a voltage-dependent capacitance. Furthermore, the properties of the charge distribution seem compatible with the idea that it accounts for the voltage-dependent capacitance which is observed experimentally. This interpretation is supported by the fact that the apparent particle valence calculated from the present capacitance measurements agrees with the valence calculated from charge movement data.

A limitation in the present experiments is that the amount of depolarization was restricted by the contraction threshold. Thus it was not possible to check the prediction of the charge movement experiments that capacitance should exhibit a maximum at $\bar{V}$, then decrease and finally become constant at very large depolarizations.

Since the charge movement underlying this component of capacitance may be involved in excitation-contraction coupling (Schneider and Chandler, 1973; Chandler et al., 1976 *b*; Adrian et al., 1976), it is of interest to calculate the amount of charge, $Q_{\text{threshold}}$, which would move at the contraction threshold, $V_{\text{threshold}}$. If Eqs. 27 and 31 apply at voltages up to $V_{\text{threshold}}$, the equation

$$Q_{\text{threshold}}/C_0 = \delta \exp [(V_{\text{threshold}} - V_{1/10})/k]/[10 \sinh (\delta/k)] \qquad (34)$$

will give the threshold charge moved, normalized according to C_0.

Calculations were carried out using a value of −48 mV for $V_{\text{threshold}}$ (Chandler et al., 1976 *b*) and values from Table II for $V_{1/10}$, k, and δ. The average value of $Q_{\text{threshold}}/C_0$ was 5.1 ± 0.7 nC/μF (mean ± SEM). If the total amount of charge Q_{MAX} is the same in isotonic as in hypertonic solution, 24.5 nC/μF (Chandler et al., 1976 *a*), then $Q_{\text{threshold}}/Q_{\text{MAX}} = 0.21 \pm 0.03$. If the sigmoid or saturating nature of the Q vs. V curve is taken into account, the estimate of $Q_{\text{threshold}}/Q_{\text{MAX}}$ is reduced to 0.18 ± 0.02. These values are in good agreement with estimates obtained from experiments on repriming contraction in depolarized fibers, 0.1–0.2 (Adrian et al., 1976).

The estimated value of −30 mV for $\bar{V}$ in the isotonic solution B, (Table II) is 14–19 mV more positive than the values −49 mV (Schneider and Chandler, 1973) and −44 mV (Chandler et al., 1976 *a*) which were found using the same solution made hypertonic with sucrose. A possible explanation of the difference is that external sucrose increases the internal ionic strength, thereby causing a decrease in the double layer potential produced by hypothetical fixed negative charges on the inner surface of the membrane.

A Second Voltage-Dependent Component of Fiber Capacitance

Fibers depolarized in 100 mM Rb solution show a component of capacitance which has different voltage-dependent properties from the component studied in normally polarized fibers. The latter component is largely or completely absent in 100 mM Rb, consistent with the fact that prolonged depolarization causes a slow decline of the charge movement currents which were discussed in

the preceding section (Chandler et al., 1976 *b*). Following Adrian and Almers (1976 *a*) we will refer to the charge movement system in depolarized fibers as charge 2 and to the charge movement in polarized fibers as charge 1.

The main differences between the effects of charge 1 and charge 2 on capacitance are the following: the extra capacitance attributed to charge 2 changes less steeply with voltage than the component attributed to charge 1 (k = 30 mV for charge 2, 12 mV for 1); the maximum increase in capacitance due to charge 2 is less than that due to charge 1 (20% for charge 2, about 50% expected for 1); the maximum in the C vs. V curve occurs at −80 to −90 mV for charge 2 as opposed to about −30 mV for charge 1 in isotonic solution.

A similarity between charge 1 and 2 is that Q_{MAX} for each process is about the same. Thus, the difference in the maximum increase in capacitance due to the two processes is simply a result of the difference in their k values.

Our results show no evidence of a voltage-dependent component of capacitance in the range $-150 < V < -100$ mV in fibers in solution B held at about −80 mV (Fig. 6). On the other hand, Adrian and Almers (1976 *a*), studying fibers held at similar potentials in hypertonic solution, have detected changes in capacitance in this voltage range. In addition, Adrian and Almers (1976 *b*) have directly observed currents due to charge 2 migration. As yet, no functional role has been assigned to charge 2.

Voltage-Dependent Changes in Capacitance due to Changes in λ_T

The first two effects of voltage on capacitance have been interpreted in terms of voltage-dependent redistribution of charges confined to the membrane phase. The third effect of voltage arises from a decrease in the space constant of the T system associated with activation of inward rectification. Going from minimum to maximum activation caused a decrease of 13–45% in the capacitance of fibers in 100 mM K solution (Table III). The decrease in tubular capacitance, obtained by subtracting the contribution of the surface membrane, was 24–55%, consistent with a mean value of 32 μm for λ_T.

If charge 2 were also present in 100 mM K solution it would have caused an increase in capacitance with hyperpolarization. Correcting for this effect by assuming that charge 2 had the same properties in 100 mM Rb and K solutions decreased the mean estimate of λ_T to 24 μm.

The dependence of capacitance on λ_T has several implications. First, in making measurements of total fiber capacitance it is important to establish that λ_T is sufficiently large to ensure that the tubular membranes are fully charged.

Second, in certain types of experiments designed to study ionic currents the degree of voltage decrement in the T system could be monitored by measuring capacitance. This might be useful in testing for radial nonuniformity under voltage clamp, both in skeletal muscle fibers and in other preparations having complicated geometries, such as cardiac or smooth muscle.

Third, an analysis of the capacitative transient can be used to localize a permeability change as being surface or tubular in origin. Experiments using fibers in 100 mM K solution indicated that 74% of the inward rectifier sites are located in the T system. If the specific capacitances of surface and tubular

membranes are the same, the result implies that the inward rectifier is evenly distributed throughout the muscle.

APPENDIX A

Effects of Electrode Leak Resistances on the Determination of Steady-State Currents

Leak Resistance at the Site of the V_1 Electrode

The presence of a leak resistance r_1 at the point of insertion of the V_1 electrode would give rise to a current loss of V_1/r_1 at $x = \ell$ and would change the functional form of the voltage distribution for $\ell < x \leq 2\ell + \ell'$. An indication of the effect of r_1 can be obtained from the lumped circuit in Fig. 2 A,

$$\frac{\Delta V}{r_i \ell} \simeq \frac{3}{2}\,\ell i_m + \frac{V_1}{r_1}\,. \tag{1 a}$$

The left side gives the current flowing across the $r_i\ell$ element whereas the right side gives the current through $3\ell y_m/2$ plus the leak current through r_1.

Eq. 1 *a* can be rearranged to give

$$i_m \simeq \frac{2\Delta V}{3r_i\ell^2} - \frac{2V_1}{3\ell r_1} \tag{2 a}$$

and can be made exact by multiplying the right side by a factor p,

$$i_m = p\left[\frac{2\Delta V}{3r_i\ell^2} - \frac{2V_1}{3\ell r_1}\right]. \tag{3 a}$$

The functional form for p can be obtained from linear cable theory. Over the segment $0 \leq x \leq \ell$ the fiber would behave as an undamaged terminated cable with voltage

$$V = V_0 \cosh\,(x/\lambda). \tag{4 a}$$

For $\ell < x \leq 2\ell + \ell'$,

$$V = A \exp\,(-x/\lambda) + B \exp\,(x/\lambda) \tag{5 a}$$

which is the general solution of Eqs. 16 and 17. The constants A and B are determined by requiring (*a*) that the values of V in Eqs. 4 *a* and 5 *a* be equal at $x = \ell$, and (*b*) that the longitudinal currents at $x = \ell$ be different by the value of current through the leak pathway. When these values for A and B are substituted into Eq. 5 *a*

$$V = V_0 \cosh\,(x/\lambda) + \frac{r_i\lambda V_0}{r_1} \cosh\,(\ell/\lambda) \sinh\,[(x - \ell)/\lambda]. \tag{6 a}$$

The factor p in Eq. 3 *a* can now be evaluated using voltage from Eq. 6 *a* and the relation $i_m = V_1/r_m$,

$$p = \frac{3}{2}\left(\frac{\ell}{\lambda}\right)^2 \frac{\cosh\,(\ell/\lambda)}{\cosh\,(2\ell/\lambda) - \cosh\,(\ell/\lambda) + K \cosh\,(\ell/\lambda)\left[\dfrac{\sinh\,(\ell/\lambda)}{\ell/\lambda} - 1\right]}. \tag{7 a}$$

K is given by the ratio $\ell r_i/r_1$. For the case where r_1 is infinite and $K = 0$ Eq. 7 *a* reduces to Eq. 8 of Adrian et al. (1970).

Although, in general, K is not known it is possible to set an upper limit to its value. From the definition of K, Eq. 3 *a* can be rewritten

$$i_m = p\left[\frac{2}{3r_i\ell^2}(\Delta V - KV_1)\right]. \tag{8 a}$$

In order for g_m to be positive, i_m must be of the same polarity as ΔV and V_1 so that $K \leq \Delta V/V_1$. For a given electrode penetration, K should be independent of g_m so that the upper bound on K is set using the minimum value of $\Delta V/V_1$ observed in that fiber. In the experiments reported here the upper bound varied from 0.01 to 0.11.

Substituting $V_1 g_m$ for i_m in Eq. 3 *a* and rearranging gives

$$\lambda = \left[\frac{2\Delta V p}{3\ell^2 V_1}\left(1 - \frac{KV_1}{\Delta V}\right)\right]^{-1/2}. \tag{9 a}$$

Values of λ calculated assuming $K = 0$ are thus underestimates if $K > 0$.

Graphs of p vs. (ℓ/λ) for $K = 0$ and $K = 0.1$ are shown in Fig. 12. For $\ell/\lambda < 0.7$ and $0 \leq K \leq 0.11$, as was the case for all experiments, $0.99 < p < 1.03$.

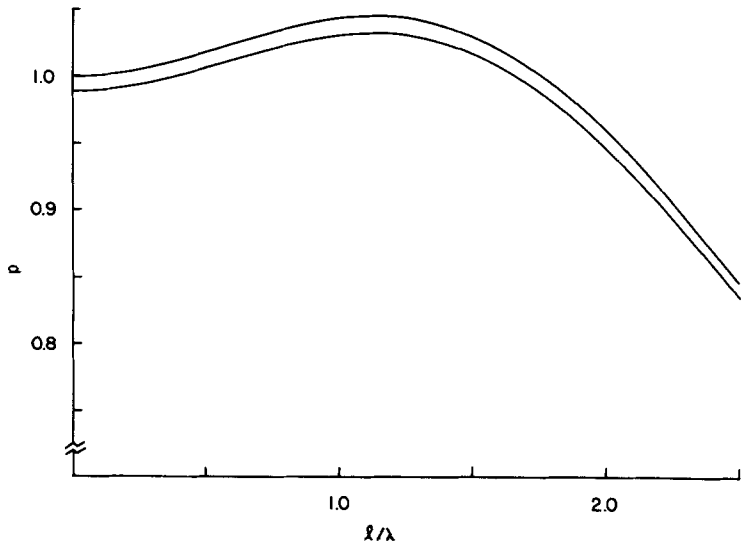

FIGURE 12. Theoretical plots of the factor p which is required to correct the lumped circuit expression for i_m. Each curve was calculated according to Eq. 7 *a*. The upper curve is for infinite r_1, $K = 0$. The lower curve is for $K = 0.1$.

EFFECT OF r_1 ON THE CURRENT ENTERING THE TERMINATED FIBER SEGMENT Another consequence of finite r_1 is that for a given value of $V_{2\ell+\ell'}$, I_S will be larger than the value predicted according to Eq. 19 for infinite r_1. Integrating Eq. 18 from $x = \ell$ to $x = 2\ell + \ell'$ gives

$$I_S^2 = 2\int_{V_1}^{V_{2\ell+\ell'}} \frac{i_m}{r_i}\, dV + I_1^2, \tag{10 a}$$

where I_1 is the current entering the point $x = \ell$ from the direction $x > \ell$. At $x = \ell$ there is a loss of current via r_1 so that

$$I_1 = I_1' + V_1/r_1, \tag{11 a}$$

where I_1' is the internal current leaving $x = \ell$ in the direction of $x < \ell$. Integrating Eq. 17 from $x = 0$ to $x = \ell$ results in

$$\left(I_1'\right)^2 = 2\int_{V_0}^{V_1} \frac{i_m}{r_i}\, dV. \tag{12 a}$$

Combining Eqs. 10 *a* through 12 *a* gives

$$I_S^2 = 2\int_{V_0}^{V_{2\ell+\ell'}} \frac{i_m}{r_i}\, dV + \frac{2V_1}{r_1}\left[2\int_{V_0}^{V_1} \frac{i_m}{r_i}\, dV\right]^{1/2} + \left[\frac{V_1}{r_1}\right]^2, \tag{13 a}$$

the expression for steady current entering the terminated segment in the presence of finite r_1.

Finite Leak Resistance at the Sites of the V_2 or I Electrodes

Presence of finite leak resistances at the points of insertion of V_2 and I electrodes will have no effect on the voltage and current distribution from $x = 2\ell$ to the end of the filter. Consequently they cannot introduce errors into calculations of λ or $r_i c_{\text{eff}}$. Since the distance ℓ' between V_2 and I electrodes is short compared with λ, it will be assumed that the sole effect of the leak resistances is to allow a loss of current equal to $V_{2\ell+\ell'}/r_2$ from the fiber at the point of insertion of the current electrode. r_2 is defined as the effective parallel resistance of the leak resistances at the V_2 and I electrodes. In this case, the total steady current applied to the fiber is given by

$$I(\infty) = I_S + I_U + V_{2\ell+\ell'}/r_2. \tag{14 a}$$

APPENDIX B

Cable Analysis for Capacitance Measurements

Using a lumped circuit (Fig. 2 A) to approximate the cable properties of the terminated fiber, c_{eff} was shown (Eq. 5) to be approximately proportional to the time integral of the transient component ΔV_{tr} of ΔV. ΔV_{tr} is given by $\Delta V - (V_1)\,[\Delta V(\infty)/V_1(\infty)]$. In this section an exact equation for calculating c_{eff} will be derived.

The derivation makes use of the Laplace transform and follows the general approach used in the Appendix of Adrian and Almers (1974). Denoting the Laplace transform of a time-varying parameter by a bar, the Laplace transform of ΔV_{tr} is given by

$$\overline{\Delta V}_{\text{tr}} = \overline{\Delta V} - \overline{V}_1 \frac{\Delta V(\infty)}{V_1(\infty)} \tag{1 b}$$

$$= \overline{V}_1\left[\frac{\overline{V}_2}{\overline{V}_1} - \frac{V_2(\infty)}{V_1(\infty)}\right].$$

By definition of the Laplace transform,

$$\overline{\Delta V}_{\text{tr}} = \int_0^\infty \Delta V_{\text{tr}} e^{-pt} dt, \tag{2 b}$$

where p is the dummy transform variable. Consequently, the time integral of ΔV_{tr} is given by

$$\int_0^\infty \Delta V_{tr} dt = \lim_{p \to 0} \Delta \bar{V}_{tr}. \tag{3 b}$$

Combining Eqs. 1 *b* and 3 *b* gives

$$\int_0^\infty \Delta V_{tr} dt = \left[\lim_{p \to 0} p\bar{V}_1\right]\left[\lim_{p \to 0} \frac{1}{p}\left\{\frac{\bar{V}_2}{\bar{V}_1} - \frac{V_2(\infty)}{V_1(\infty)}\right\}\right]. \tag{4 b}$$

To measure capacitance a voltage change V_2 is applied at $x = 2\ell$ for a sufficiently long time so that both V_2 and V_1 reach steady levels, $V_2(\infty)$ and $V_1(\infty)$. Consequently,

$$\lim_{p \to 0} p\bar{V}_1 = V_1(\infty), \tag{5 b}$$

$$\lim_{p \to 0} p\bar{V}_2 = V_2(\infty), \tag{6 b}$$

and

$$\lim_{p \to 0} \bar{V}_2/\bar{V}_1 = V_2(\infty)/V_1(\infty). \tag{7 b}$$

The MacLaurin's series for $\bar{V}_2/\bar{V}_1$ can thus be expressed as

$$\frac{\bar{V}_2}{\bar{V}_1} = \frac{V_2(\infty)}{V_1(\infty)} + p\frac{\mathrm{d}}{\mathrm{d}p}\left(\frac{\bar{V}_2}{\bar{V}_1}\right) + \frac{p^2}{2!}\frac{\mathrm{d}^2}{\mathrm{d}p^2}\left(\frac{\bar{V}_2}{\bar{V}_1}\right) + \ldots\ , \tag{8 b}$$

where the derivatives are evaluated at $p = 0$.

Eq. 8 *b* can be rearranged and limits taken to give

$$\lim_{p \to 0}\left[\frac{1}{p}\left\{\frac{\bar{V}_2}{\bar{V}_1} - \frac{V_2(\infty)}{V_1(\infty)}\right\}\right] = \lim_{p \to 0} \frac{\mathrm{d}}{\mathrm{d}p}\left(\frac{\bar{V}_2}{\bar{V}_1}\right). \tag{9 b}$$

Substituting Eqs. 5 *b* and 9 *b* into 4 *b* gives

$$\int_0^\infty \Delta V_{tr} dt = V_1(\infty) \lim_{p \to 0} \frac{\mathrm{d}}{\mathrm{d}p}\left(\frac{\bar{V}_2}{\bar{V}_1}\right). \tag{10 b}$$

Since $\bar{V}_1$ and $\bar{V}_2$ appear only as the ratio $\bar{V}_2/\bar{V}_1$ in Eq. 10 *b*, any delays in recording V_1 and V_2 will introduce errors into the measured value of the ΔV_{tr} integral only if the delays are not the same. This follows from the fact that the recorded voltages V_1' and V_2' are related to the actual voltages V_1 and V_2 by $\bar{V}_1' = f_1(p)\bar{V}_1$ and $\bar{V}_2' = f_2(p)\bar{V}_2$, $f_1(p)$ and $f_2(p)$ being transfer functions. If the delays are identical for V_1 and V_2, $f_1(p)$ and $f_2(p)$ are equal and $\bar{V}_2'/\bar{V}_1' = \bar{V}_2/\bar{V}_1$. For this reason the microelectrodes for V_1 and V_2 were selected to have the same resistance and amplifiers A_1 and A_2 were identical in design.

The expressions for $\bar{V}_1$ and $\bar{V}_2$ to be used with Eq. 10 *b* can be obtained directly from the DC steady-state equations for V_1 and V_2 by substituting the fiber admittance function y_m for g_m and by using $\bar{V}_1$ and $\bar{V}_2$, respectively, in place of V_1 and V_2. Following these substitutions the fiber propagation constant γ, defined as $(r_i y_m)^{1/2}$, appears in place of each $1/\lambda$ term in the DC equations. For the circuit in Fig. 2 B,

$$y_m = g_m + pc_m' + \sum_{n=1}^{\infty} \frac{pc_n}{1 + pr_n c_n}, \tag{11 b}$$

where r_n and c_n represent the resistance and capacitance of the nth series RC element. Note that for $p \to 0$, $y_m \to g_m$ and $\gamma \to 1/\lambda$.

Case I: Infinite Leak Resistance at the V_1 Electrode

For the case of infinite leak resistance r_1 at the site of insertion of the V_1 electrode, the equation for $\bar{V}_2/\bar{V}_1$ is obtained from the corresponding steady-state equation as

$$\frac{\bar{V}_2}{\bar{V}_1} = \frac{\cosh 2\gamma\ell}{\cosh\gamma\ell} \cdot \tag{12 b}$$

Consequently,

$$\lim_{p\to 0}\left[\frac{d}{dp}\left(\frac{\bar{V}_2}{\bar{V}_1}\right)\right] = \lim_{p\to 0}\left[\frac{d}{d\gamma}\left(\frac{\cosh 2\gamma\ell}{\cosh\gamma\ell}\right)\frac{d\gamma}{dy_m}\frac{dy_m}{dp}\right]. \tag{13 b}$$

Since

$$\lim_{p\to 0}\frac{dy_m}{dp} = c_m' + \sum_{n=1}^{\infty} c_n \tag{14 b}$$

$$= c_{\text{eff}}$$

and

$$\lim_{p\to 0}\frac{d\gamma}{dy_m} = \frac{r_i\lambda}{2}, \tag{15 b}$$

$$\lim_{p\to 0}\frac{d}{dp}\left(\frac{\bar{V}_2}{\bar{V}_1}\right) = \frac{2\ell\cosh(\ell/\lambda)\sinh(2\ell/\lambda) - \ell\cosh(2\ell/\lambda)\sinh(\ell/\lambda)}{\cosh^2(\ell/\lambda)}\left(\frac{r_i\lambda c_{\text{eff}}}{2}\right). \tag{16 b}$$

Substituting into Eq. 10 *b* and rearranging yields

$$c_{\text{eff}} = \frac{2h(\ell/\lambda)}{3\ell^2 r_i V_1(\infty)}\int_0^{\infty}\Delta V_{\text{tr}}dt, \tag{17 b}$$

similar to Eq. 6.

The function $h(\ell/\lambda)$, defined as

$$h(\ell/\lambda) = \frac{3\ell}{\lambda}\left[\frac{\cosh^2(\ell/\lambda)}{2\cosh(\ell/\lambda)\sinh(2\ell/\lambda) - \cosh(2\ell/\lambda)\sinh(\ell/\lambda)}\right], \tag{18 b}$$

is the factor which, when multiplied by the approximate expression for c_{eff} (Eq. 5), makes it exact. A graph of h as a function of ℓ/λ for the case of infinite r_1 is presented as the upper curve in Fig. 4.

Case II: Finite Leak Resistance at the V_1 Electrode

For the case of finite r_1, V_2/V_1 is obtained by using Eq. 6 *a* for $V_2(\infty)$ and Eq. 4 *a* for $V_1(\infty)$, giving

$$\frac{V_2(\infty)}{V_1(\infty)} = \frac{\cosh(2\ell/\lambda)}{\cosh(\ell/\lambda)} + \frac{K\lambda}{\ell}\sinh(\ell/\lambda), \tag{19 b}$$

and

$$\frac{\bar{V}_2}{\bar{V}_1} = \frac{\cosh 2\gamma\ell}{\cosh\gamma\ell} + K\frac{\sinh\gamma\ell}{\gamma\ell}. \tag{20 b}$$

The first term in Eq. 20 *b* constitutes the complete equation for the case of infinite r_1; the limit as $p \to 0$ of its derivative with respect to p is given in Eq. 16 *b*. Considering the second term,

$$\lim_{p\to 0} \frac{d}{dp}\left(\frac{K \sinh \gamma\ell}{\gamma\ell}\right) = K\left[\lambda \cosh(\ell/\lambda) - \frac{\lambda^2}{\ell}\sinh(\ell/\lambda)\right]\left(\frac{r_i \lambda c_{eff}}{2}\right). \quad (21\,b)$$

Using the sum of Eqs. 16 *b* and 21 *b* for the limit term in Eq. 10 *b* and rearranging, an equation identical to Eq. 17 *b* is obtained, except that now the correction factor $h(\ell/\lambda)$ is given by

$$h(\ell/\lambda) = \frac{3\ell}{\lambda}\left[\frac{2\cosh(\ell/\lambda)\sinh(2\ell/\lambda) - \cosh(2\ell/\lambda)\sinh(\ell/\lambda)}{\cosh^2(\ell/\lambda)} + K(\lambda/\ell)\cosh(\ell/\lambda) - K(\lambda/\ell)^2\sinh(\ell/\lambda)\right]^{-1}. \quad (22\,b)$$

In this case h is a function of K as well as of ℓ/λ. The lower curve in Fig. 4 is a graph of $h(\ell/\lambda)$ for $K = 0.1$.

If r_1 is assumed to be infinite, when in fact it is not, two errors are introduced into the calculation of $h(\ell/\lambda)$. First, the value of $h(\ell/\lambda)$ would be too large because the $K = 0$ curve is used rather than the curve corresponding to the correct value of K (see Fig. 4). Second, the value of ℓ/λ used for calculating $h(\ell/\lambda)$ would be overestimated (Eq. 9 *a*). Since the calculated value of ℓ/λ was always less than 0.7, the portion of the $h(\ell/\lambda)$ curve of interest increases monotonically with ℓ/λ. Thus the overestimate of ℓ/λ would lead to an additional increase in $h(\ell/\lambda)$. The combined error in determining $h(\ell/\lambda)$ under the conditions of the experiments ($K \leq 0.11$, $\ell/\lambda < 0.7$) was at most 2.5%.

We thank Mr. Harry Fein and staff of the electronic and machine shop for help with the design and construction of equipment. The computer of average transients was lent by Dr. J. M. Ritchie. We are grateful to Dr. R. W. Tsien for helpful discussion and for reading the manuscript, to Mrs. Lillian Peracchia for preparing the figures, and to Miss Denise Yetto for expert typing of several versions of the manuscript.

Financial support was provided by United States Public Health Services Grant NS 05477.

Received for publication 7 July 1975.

REFERENCES

ADRIAN, R. H. 1964. The rubidium and potassium permeability of frog muscle membrane. *J. Physiol. (Lond.).* **175**:134–159.

ADRIAN, R. H., and W. ALMERS. 1974. Membrane capacity measurements on frog skeletal muscle in media of low ionic content. *J. Physiol. (Lond.).* **237**:573–606.

ADRIAN, R. H., and W. ALMERS. 1976 *a*. The voltage dependence of membrane capacity. *J. Physiol. (Lond.).* In press.

ADRIAN, R. H., and W. ALMERS. 1976 *b*. Charge movement in the membrane of striated muscle. *J. Physiol. (Lond.).* In press.

ADRIAN, R. H., W. K. CHANDLER, and A. L. HODGKIN. 1969. The kinetics of mechanical activation in frog muscle. *J. Physiol. (Lond.).* **204**:207–230.

ADRIAN, R. H., W. K. CHANDLER, and A. L. HODGKIN. 1970 *a*. Voltage clamp experiments in striated muscle fibres. *J. Physiol. (Lond.).* **208**:607–644.

ADRIAN, R. H., W. K. CHANDLER, and A. L. HODGKIN. 1970 *b*. Slow changes in potassium permeability in skeletal muscle. *J. Physiol. (Lond.).* **208**:645–668.

ADRIAN, R. H., W. K. CHANDLER, and R. F. RAKOWSKI. 1976. Charge movement and mechanical repriming in skeletal muscle. *J. Physiol. (Lond.).* In press.

ADRIAN, R. H., and W. H. FREYGANG. 1962. The potassium and chloride conductance of frog muscle membrane. *J. Physiol. (Lond.).* **163**:61–103.

ALMERS, W. 1972 *a*. Potassium conductance changes in skeletal muscle and the potassium concentration in the transverse tubules. *J. Physiol. (Lond.).* **225**:33–56.

ALMERS, W. 1972 *b*. The decline of potassium permeability during extreme hyperpolarization in frog skeletal muscle. *J. Physiol. (Lond.).* **225**:57–83.

ALMERS, W. 1975. Observations on intramembrane charge movements in skeletal muscle. *Philos. Trans. R. Soc. Lond. B Biol. Sci.* **270**:507–513.

ALMERS, W. 1976. Some dielectric properties of muscle membrane and their possible importance for excitation-concentration coupling. *Ann. N. Y. Acad. Sci.* In press.

BODE, H. W. 1938. Impedance and energy relations in electrical networks. *Physica.* **5**:143–144.

CHANDLER, W. K., R. F. RAKOWSKI, and M. F. SCHNEIDER. 1976 *a*. A nonlinear voltage dependent charge movement in frog skeletal muscle. *J. Physiol. (Lond.).* In press.

CHANDLER, W. K., R. F. RAKOWSKI, and M. F. SCHNEIDER. 1976 *b*. Effects of glycerol treatment and maintained depolarization on charge movement in skeletal muscle. *J. Physiol. (Lond.).* In press.

CHANDLER, W. K., and M. F. SCHNEIDER. 1976. Time-course of potential spread along a skeletal muscle fiber under voltage clamp. *J. Gen. Physiol.* **67**:165.

CHANDLER, W. K., M. F. SCHNEIDER, R. F. RAKOWSKI, and R. H. ADRIAN. 1975. Charge movements in skeletal muscle. *Philos. Trans. R. Soc. Lond. B Biol. Sci.* **270**:501–505.

COLE, K. S., and H. J. CURTIS. 1941. Membrane potential of the squid axon during current flow. *J. Gen. Physiol.* **24**:551–563.

COLE, K. S. 1968. Membranes, Ions and Impulses. University of California Press, Berkeley, Calif.

EISENBERG, R. S., and P. W. GAGE. 1969. Ionic conductances of the surface and transverse tubular membranes of frog sartorius fibers. *J. Gen. Physiol.* **53**:279–297.

EISENBERG, R. S., and E. A. JOHNSON. 1970. Three dimensional field problems in physiology. *Prog. Biophys. Mol. Biol.* **20**:1–65.

FALK, G., and P. FATT. 1964. Linear electrical properties of striated muscle fibres observed with intracellular electrodes. *Proc. R. Soc. B Biol. Sci.* **160**:69–123.

FATT, P., and B. KATZ. 1951. An analysis of the end-plate potential recorded with an intracellular electrode. *J. Physiol. (Lond.).* **115**:320–370.

GOMORI, G. 1955. Preparation of buffers for use in enzyme studies. *In* Methods in Enzymology. S. P. Colowick and N. O. Kaplan, editors. Academic Press, Inc., New York. **1**:138–146.

HODGKIN, A. L., and P. HOROWICZ. 1959. The influence of potassium and chloride ions on the membrane potential of single muscle fibres. *J. Physiol. (Lond.).* **148**:127–160.

HODGKIN, A. L., and P. HOROWICZ. 1960. The effect of sudden changes in ionic concentrations on the membrane potential of single muscle fibres. *J. Physiol. (Lond.).* **153**:370–385.

HODGKIN, A. L., and S. NAKAJIMA. 1972 *a*. The effect of diameter on the electrical constants of frog skeletal muscle fibres. *J. Physiol. (Lond.).* **221**:105–120.

HODGKIN, A. L., and S. NAKAJIMA. 1972 *b*. Analysis of the membrane capacity in frog muscle. *J. Physiol. (Lond.).* **221**:121–136.

HUTTER, O. F., and D. NOBLE. 1960. The chloride conductance of frog skeletal muscle. *J. Physiol. (Lond.).* **151**:89–102.

KATZ, B. 1948. The electrical properties of the muscle fibre membrane. *Proc. R. Soc. B Biol. Sci.* **135**:506–534.

KATZ, B. 1949. Les constantes électrique de la membrane du muscle. *Arch. Sci. Physiol.* **3**:285–300.

MOBLEY, B. A., J. LEUNG, and R. S. EISENBERG. 1974. Longitudinal impedance of skinned frog muscle fibers. *J. Gen. Physiol.* **63**:625–637.

MOBLEY, B. A., J. LEUNG, and R. S. EISENBERG. 1975. Longitudinal impedance of single frog muscle fibers. *J. Gen. Physiol.* **65**:97–113.

SCHNEIDER, M. F. 1970. Linear electrical properties of the transverse tubules and surface membrane of skeletal muscle fibers. *J. Gen. Physiol.* **56**:640–671.

SCHNEIDER, M. F., and W. K. CHANDLER. 1973. Voltage dependent charge movement in skeletal muscle: a possible step in excitation-contraction coupling. *Nature (Lond.).* **242**:244–246.

STANFIELD, P. R. 1970. The effect of tetraethylammonium ion on the delayed currents of frog skeletal muscle. *J. Physiol. (Lond.).* **209**:209–229.

VALDIOSERA, R., C. CLAUSEN, and R. S. EISENBERG. 1974 *a*. Measurement of the impedance of frog skeletal muscle fibers. *Biophys. J.* **14**:295–315.

VALDIOSERA, R., C. CLAUSEN, and R. S. EISENBERG. 1974 *b*. Impedance of frog skeletal muscle fibers in various solutions. *J. Gen. Physiol.* **63**:460–491.

WARNER, A. E. 1972. Kinetic properties of the chloride conductance of frog muscle. *J. Physiol. (Lond.).* **227**:291–312.